Accepted Manuscript

Donepezil-like Multifunctional Agents: Design, Synthesis, Molecular Modeling and Biological Evaluation

Ming-Yu Wu, Gerard Esteban, Simone Brogi, Masahi Shionoya, Li Wang, Giuseppe Campiani, Mercedes Unzeta, Tsutomu Inokuchi, Stefania Butini, Jose Marco-Contelles

Please cite this article as: M.-Y. Wu, G. Esteban, S. Brogi, M. Shionoya, L. Wang, G. Campiani, M. Unzeta, T. Inokuchi, S. Butini, J. Marco-Contelles, Donepezil-like Multifunctional Agents: Design, Synthesis, Molecular Modeling and Biological Evaluation, *European Journal of Medicinal Chemistry* (2015), doi: 10.1016/j.ejmech.2015.10.001.

Donepezil-like Multifunctional Agents: Design, Synthesis, Molecular Modeling and Biological Evaluation

Ming-Yu Wu,[a,§] Gerard Esteban,[b,§] Simone Brogi,[c,§] Masahi Shionoya,[a] Li Wang,[a] Giuseppe Campiani,[c] Mercedes Unzeta,[b,*] Tsutomu Inokuchi,[a,*] Stefania Butini,[c,*] and Jose Marco-Contelles[d,*]

[a]*Division of Chemistry and Biotechnology, Graduate School of Natural Science and Technology, Okayama University, 3.1.1 Tsushima-Naka, Kita-ku, Okayama 700-8530, Japan.*

[b]*Departament de Bioquímica i Biologia Molecular, Facultat de Medicina, Institut de Neurociències, Universitat Autònoma de Barcelona, 08193 Bellaterra, Barcelona, Spain.*

[c]*European Research Centre for Drug Discovery and Development (NatSynDrugs) and Department of Biotechnology, Chemistry and Pharmacy, Università degli Studi di Siena Via A. Moro, 53100 Siena, Italy.*

[d]*Laboratory of Medicinal Chemistry (IQOG, CSIC), C/Juan de la Cierva 3, 28006-Madrid, Spain.*

[*]Corresponding author. Tel. +34 93 5811523; fax +34 935811573; e-mail: mercedes.unzeta@uab.cat

[*]Corresponding author. Tel. +81862945045; fax +81862518021; e-mail: inokuchi@cc.okayama-u.ac.jp

[*]Corresponding author. Tel.: +39 0577234161; fax: +39 0577 234254; e-mail: butini3@unisi.it

[*]Corresponding author. Tel.: + 34 915622900; fax: +39 915644853; e-mail: iqoc21@iqog.csic.es

[§]Authors equally contributed to this work

Abstract

Currently available drugs against Alzheimer's disease (AD) are only able to ameliorate the disease symptoms resulting in a moderate improvement in memory and cognitive function without any efficacy in preventing and inhibiting the progression of the pathology. In an effort to obtain disease-modifying anti-Alzheimer's drugs (DMAADs) following the multifactorial nature of AD, we have recently developed multifunctional compounds. We herein describe the design, synthesis, molecular modeling and biological evaluation of a new series of donepezil-related compounds possessing metal chelating properties, and being capable of targeting different enzymatic systems related to AD (cholinesterases, ChEs, and monoamine oxidase A, MAO-A). Among this set of analogues compound **5f** showed excellent ChEs inhibition potency and a selective MAO-A inhibition (vs MAO-B) coupled to strong complexing properties for zinc and copper ions, both known to be involved in the progression of AD. Moreover, **5f** exhibited moderate antioxidant properties as found by *in vitro* assessment. This compound represents a novel donepezil-hydroxyquinoline hybrid with DMAAD profile paving the way to the development of a novel class of drugs potentially able to treat AD.

1. Introduction

Alzheimer's disease (AD) represents the most prevalent pathology associated to neurodegenerative senile dementia, characterized by selective loss of cholinergic neurons and reduced level of acetylcholine (ACh) neurotransmitter, driving to memory deficit and progressive impairment of cognitive functions up to debilitating dementia before death [1, 2]. This pathology has been found to be related to many factors including ACh levels, β-amyloid plaques deposition, oxidative damage, free radicals formation and metal ions [3-6]. AD currently affects millions of aging people (WHO report 2012, Dementia: a public health priority) [7], a number which, with the greying of society, will lead to a dramatic increase expecting a double of patients by 2030 and triple by 2050 [8]. To date, healthcare or financial systems in developed countries are not prepared to manage this worrisome scenario [7]. Indeed the only available therapeutics for AD, focused on increasing cholinergic neurotransmission in the brain (by inhibiting cholinesterases, ChEs), have resulted in a modest improvement in memory and cognitive function and are devoid of any therapeutic potential concerning prevention and progression of neurodegeneration [9]. All the currently registered drugs for the treatment of AD are ChEIs (donepezil, **1**, rivastigmine, **2**, and galantamine, **3**, Figure 1). The *N*-methyl-*D*-aspartate (NMDA) antagonist memantine was approved for the treatment of moderate to severe AD [10, 11], while tacrine, **4** (Figure 1) the first drug approved for the treatment of AD, was withdrawn from the market [12] due to its hepatotoxicity [13, 14]. The narrowness of therapies for AD has become as the current biggest unmet medical need in neurology unless an effective disease-modifying anti-Alzheimer's drug (DMAAD) is found [15].
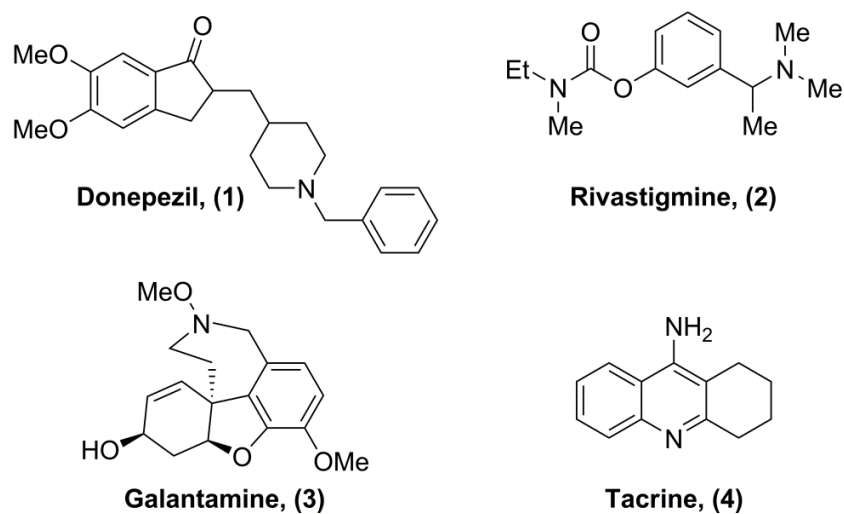
Figure 1 Current cholinesterase inhibitors approved for the treatment of AD.

The multifactorial nature of AD has led to "the failure of the so-called *one-drug-one-target* paradigm" [16, 17]. Besides the well-recognized symptomatic efficacy of ChEs inhibition for the treatment of AD a therapeutic potential was proposed for monoamine oxidase inhibitors (MAOIs). Indeed, among the factors that may contribute to cell death in neurodegenerative disorders such as AD, oxidative stress plays a relevant role. MAOIs can reduce the formation of neurotoxic products such as H_2O_2 and aldehydes, which in turn, promote the generation of reactive oxygen species (ROS) [18], endorsing MAOIs with strong neuroprotective properties [19].

Amyloid beta (Aβ) aggregation and Aβ ☐plaques formation represent the hallmarks of AD. The amyloid cascade hypothesis of AD postulates that excessive Aβ formation is one of the causes of neurodegeneration. Furthermore, the metallostasis evidence points to iron, copper and zinc as relevant metals in the pathogenesis of AD, either by direct interaction with Aβ, thus increasing its aggregation, or by enhancing the production of H_2O_2 and ROS. Consequently, the modulation of the homeostasis of these biometals is a potential therapeutic strategy for AD therapy [20]. In healthy people amyloid precursor protein and Aβ interact with the mentioned metal species in a subtle equilibrium. Disruption

of this balance drives to an abnormal Aβ metabolism as well as an alteration in copper and zinc uptake, leading to the formation of Aβ fibrils. The formation of fibrils may induce an inflammatory reaction with consequent decrease of pH, also modifying the zinc homeostasis [21]. Zinc is thus released into the cellular environment triggering the events that lead to oxidative stress-induced cell death. Copper ions are then free to compete for zinc binding site on Aβ, and these ions can catalyse H_2O_2 production by Aβ. As a consequence of the inflammatory response, a highly reactive free radical, nitric oxide is released to regulate the process [22].

Accordingly, in the last years the multifactorial etiology of AD has driven the research to develop novel multitarget anti-AD agents [23-28]. In this frame, we have previously explored: i) multifunctional compounds able to inhibit both ChEs [29-31], ii) compounds with multifunctional profile coupling the inhibition of ChEs with Aβ aggregation as well as with the disruption of preformed fibrils [32, 33], iii) compounds with acetylcholinesterase (AChE) and MAOs inhibition capacity [34, 35], and iv) compounds with AChE and MAOs inhibition capacity showing additional antioxidant properties [36, 37]. Based on our knowledge and by a scaffold hopping approach, we herein report the development of novel chemical entities (compounds **5a-f**, Figure 2) which represent an improved series of our previously developed analogues typified by **DPH6** (Table 1) [38]. Compounds **5a-f** combine the *N*-benzylpiperidine moiety of **1** with a metal chelating portion represented by a 8-hydroxyquinoline system functionalized at position 2. Since **1** is a weak MAO-B inhibitor and is devoid of MAO-A affinity, for improving the MAO inhibition properties of the compounds, we also introduced the propargylamine moiety.
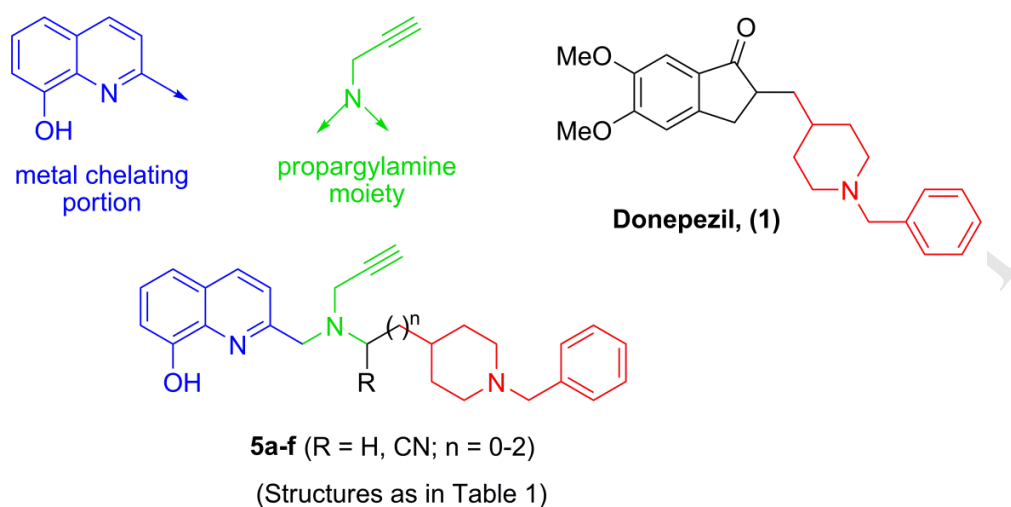
Figure 2. Design of the title compounds **5a-f**.

Pharmacological analysis revealed the developed compounds as potent AChE and butyrylcholinesterase (BuChE) inhibitors, with IC_{50} values in the nanomolar range combined with micromolar MAO-A selective inhibition (*vs* MAO-B), metal-chelating capability and moderate antioxidant properties. In-depth bioinformatics analysis of the analogues with AChE BuChE and MAO-A and -B helped rationalizing the observed enzyme inhibition data. Among the analogues described, compound **5f** showed the most interesting profile as multifuntional tool, thus representing an innovative scaffold for the development of improved donepezil-hydroxyquinoline hybrids as potential DMAADs.

2. Results and Discussion

2.1. Chemistry

To obtain the compounds presented in this paper the following synthetic schemes 1-3 were adopted.

ω-(1-Benzylpiperidin-4-yl)alkanals **10a,b** were prepared in our previous methods [38]. Thus, two-carbon homologation of the commercial ketone **6a** and aldehyde **6b** with Horner-Wadsworth-Emmons reagent **7** (derived from Arbuzov reaction between triethyl phosphite and 1-chloroacetonitrile) gave **8a,b**. On the latter olefins double bond reduction with Mg-I_2 in MeOH followed by DIBAL-H reduction of the resulting alkanenitriles **9a,b** gave the correspondent aldehydes **10a,b** (Scheme 1).

The secondary amine, *N*-(2-propynyl)-*N*-(quinolin-2-yl)methylamine, **14** was prepared by reductive amination of the quinoline-2-carbaldehyde **13** with propargylamine, using $NaBH_4$ under acidic conditions. For this process, **13** was derived from commercially available 2-methylquinolin-8-ol (**11**) by SeO_2 oxidation followed by silylation of **12** with TBSCl (Scheme 2).

Reductive amination of **6b** and ω-(1-benzylpiperidin-4-yl)alkanals **10a,b** with the secondary amine **14**, using $NaBH_4$ under acidic conditions, afforded two component coupled tertiary amines **15a-c**, which were desilylated by treatment with Bu_4NF to give the desired donepezil + propargylamine + 8-hydroxyquinoline hybrid compounds (DPHs) **5a-c** (Scheme 3). DPHs **5d-f** were prepared in short synthetic sequences through Lewis acid-catalyzed Strecker reaction as the key operation [39]. Thus, the aldehydes **6a**, **10a** and **10b** were treated with TMSCN in the presence of ZnI_2, forming the corresponding cyanohydrin TMS ethers **16a-c**, which was immediately followed by addition of the secondary amine **14** to give the corresponding α-aminonitriles **17a-c**, respectively. Finally, the TBS-protective group of **17a-c** was removed by treatment with Bu_4NF in THF, affording the desired DPHs **5d-f** (Scheme 3). All new molecules showed analytical and spectroscopic data in good agreement with their structures, and then submitted to biological evaluation as racemic mixtures.
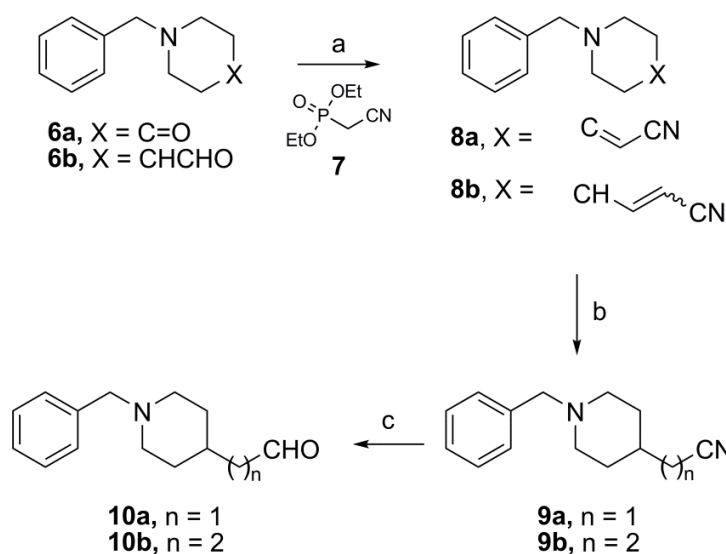
Scheme 1. Synthesis of aldehydes 10a,b. Reagents and conditions: (a) K$_2$CO$_3$, THF, rt–reflux; (b) Mg/I$_2$, MeOH, 0 °C, rt; (c) DIBAL-H/toluene, -78 °C.
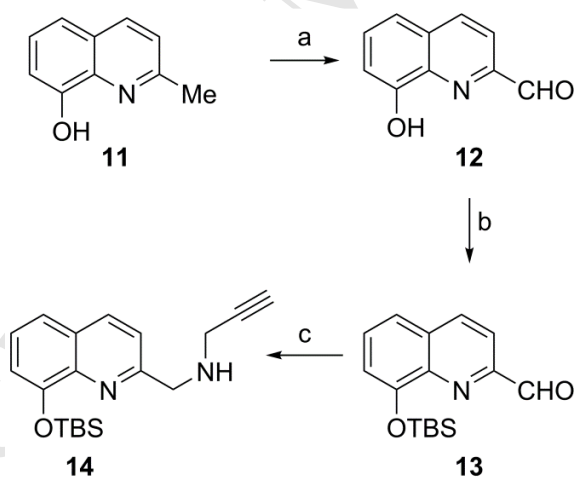
Scheme 2. Synthesis of intermediate amine 14. Reagents and conditions: (a) SeO$_2$/1,4-dioxane, 60 °C–reflux; (b) propargylamine, imidazole, TBSCl/DCM, 0 °C–rt; (c) CF$_3$COOH/MeOH, 0 °C–rt then NaBH$_4$, 0 °C–rt.
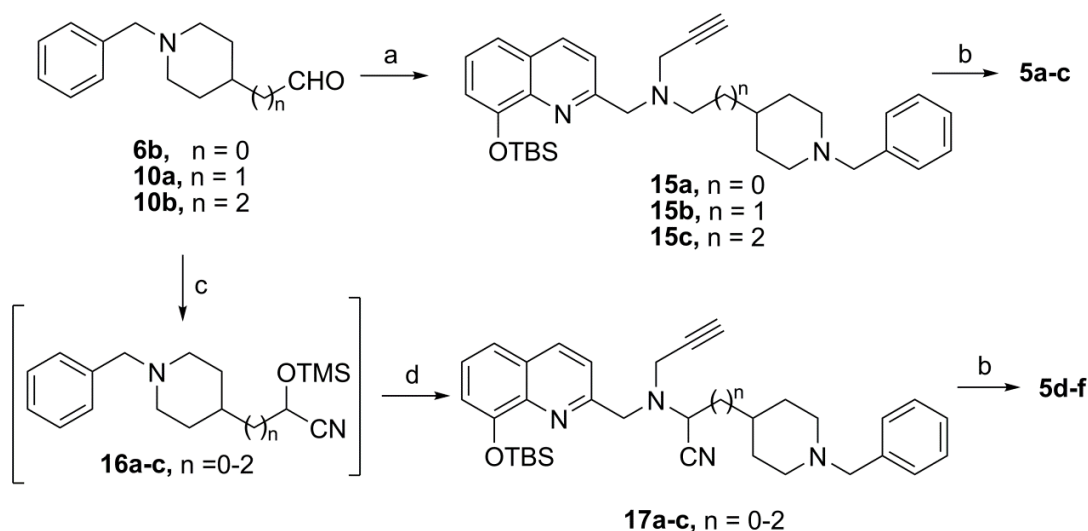
Scheme 3. Synthesis of title compounds 5a-f. Reagents and conditions: (a) compound **14**, CF$_3$CO$_2$H/MeOH, 0 °C–rt then NaBH$_4$, 0 °C–rt; (b) TBAF/THF, rt; (c) TMSCN, ZnI$_2$/DCM, rt; (d) compound **14**, MeOH, 50 °C, 3 h.
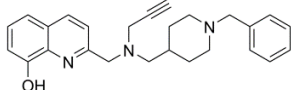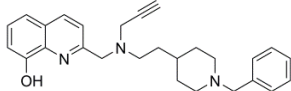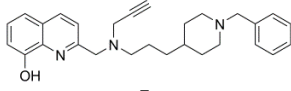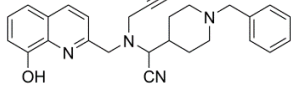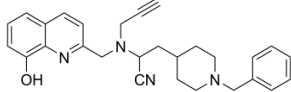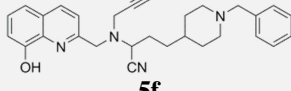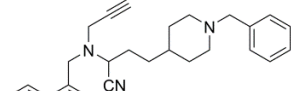
2.2. Pharmacological evaluation, structure‑activity relationship, and molecular modeling studies

2.2.1. Enzyme assays

Donepezil (Aricept®) is an AChE inhibitor able to increase concentrations of ACh in the brain and improving the symptoms of disease without delaying the progression of AD. Donepezil was approved by the FDA in 1996 with the trade name of Aricept® and in 2006 the drug was also approved for treating severe dementia. As shown in Table 1, donepezil displayed an IC$_{50}$ value in the nanomolar range regarding AChE activity inhibition with weak selectivity for other enzymatic systems (BuChE and MAOs). In an effort to design multifunctional compounds as DMAADs the benzyl-piperidine moiety of donepezil and 8-hydroxyquinoline nucleus, were combined for maintaining both the ChEs inhibitory activity and metal-chelating properties. A propargylamine moiety for inhibiting MAO was also inserted between these two moieties by a carbon chain of variable length. This approach led to the

design of compounds **5a**-**f** (Figure 2 and Table 1). Further in compounds **5d-f** the spacer was decorated with a cyano group as a further interacting group for potentiating enzyme inhibition. The obtained compounds were evaluated *in vitro* for assessing their inhibition properties at the human enzymes of interest (MAO-A, MAO-B, AChE, and BuChE). As shown in Table 1 the compound **5f** exhibited the most interesting profile of the series. In fact, **5f** inhibited AChE activity in the nanomolar range with an IC_{50} value of 29 nM, similar to that found for **1**. Furthermore, our prototypic multifunctional compound **5f** showed an excellent inhibitory potency (IC_{50} = 39 nM) against the BuChE being more potent than reference compound **1** (IC_{50} = 7.5 μM). In addition **5f** was found to be a selective MAO-A (vs MAO-B) inhibitor in the micromolar range (IC_{50} = 10.1 μM), whereas **1** did not show appreciable MAO-A inhibitory activity and displayed MAO-B inhibition potency in the micromolar range (IC_{50} = 15.2 μM). **DPH6** (Table 1) [38], the progenitor molecule of all these compounds, when compared with **5f**, it showed similar IC_{50} values versus MAO-A, but higher affinity versus MAO-B and lower inhibition potency towards AChE and BuChE. Taken into account these data, we can assess that compound **5f** nicely challenged the *in vitro* profile of **DPH6**.

Table 1. Inhibitory activities (IC$_{50}$) and selectivity ratios of derivatives inhibiting *human recombinant* MAO (*hr*MAO) isoforms and *human recombinant* ChEs.

Compound	IC$_{50}$ (µM)[a]			IC$_{50}$ (µM)[a]		
	*hr*MAO-A	*hr*MAO-B	SI[b]	*hr*AChE	*hr*BuChE	SI[c]
5a	46.5 ± 4.4	>100	>2.2	9.7 ± 1.0	0.064 ± 0.005	152
5b	35.6 ± 3.7	>100	>2.8	4.1 ± 0.6	0.079 ± 0.013	52
5c	37.0 ± 3.8	>100	>2.7	1.5 ± 0.2	0.023 ± 0.003	65
5d	10.2 ± 1.2	>100	>9.8	64.2 ± 7.1	0.030 ± 0.004	2140
5e	12.2 ± 1.3	>100	>8.2	3.3 ± 0.6	0.002 ± 0.0003	1650
5f	**10.1 ± 1.1**	**>100**	**>9.9**	**0.029 ± 0.003** / **0.015 ± 0.004** (Ki)	**0.039 ± 0.003** / **0.052 ± 0.002** (Ki)	**0.7** / **2.9**
Clorgyline	0.016 ± 0.003	65.5 ± 7.1	4094	>500	>500	-
***l*-Deprenyl**	55.4 ± 6.5	0.02 ± 0.003	0.0004	>500	>500	-
1 (Donepezil)	>1000	15.2 ± 1.7	<0.0152	0.009 ± 0.001	7.5 ± 0.8	0.0012
DPH6	6.7 ± 0.8	11.8 ± 1.5	1.8	0.35 ± 0.11	2.1± 0.2	0.17

[a]Values obtained after 30 min pre-incubation expressed as the mean ± S.E.M. of at least three independent experiments. [b]MAO-A selectivity index: [IC$_{50}$(*hr*MAO-B)]/[IC$_{50}$(*hr*MAO-A)]. [c]*hr*BuChE selectivity index: [IC$_{50}$(*hr*BuChE)]/[IC$_{50}$(*hr*AChE)].

In order to provide some relevant information about the mechanism of action of **5f**, an assessment to establish the reversibility and time-dependent inhibition of hrMAO-A and hrChEs was performed. In Figure 3 the output of these *in vitro* studies concerning MAO-A is shown.
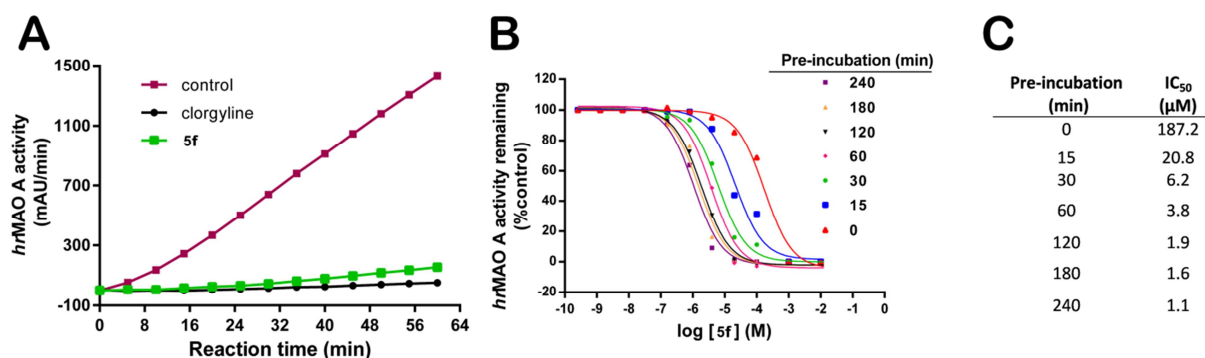
Figure 3. Assessment for reversibility and time-dependent inhibition of hrMAO-A by derivative **5f**. A) hrMAO-A activity was measured after a 30 min pre-incubation with either still water as a control, 100 μM **5f** or 200 nM clorgyline (10-fold of the IC$_{50}$ values) and followed by a large dilution of the enzyme-inhibitor complex; B) dose-response curves of hrMAO-A inhibited by a **5f** performed at different pre-incubation times (0-240 min); C) IC$_{50}$ values determined from dose-response curves of hrMAO-A inhibition by **5f** after different pre-incubations.

Unequivocally, the lack of recovery of activity after enzyme inactivation by **5f** (Figure 3A) confirms an irreversible MAO-A inhibition similarly to that observed with the reference inhibitor clorgyline. This result is consistent with the covalent interaction between the propargylamine moiety and the flavin adenine dinucleotide (FAD) co-factor present in the MAO-A enzyme. This type of inhibition is also in agreement with molecular modelling studies discussed below (see paragraph 2.2.2 for further details). Moreover, a time-dependent inhibition mechanism of hrMAO-A (Figure 3B and 3C) was evidenced from the dose-response curves (IC$_{50}$) when different pre-incubations times were employed.
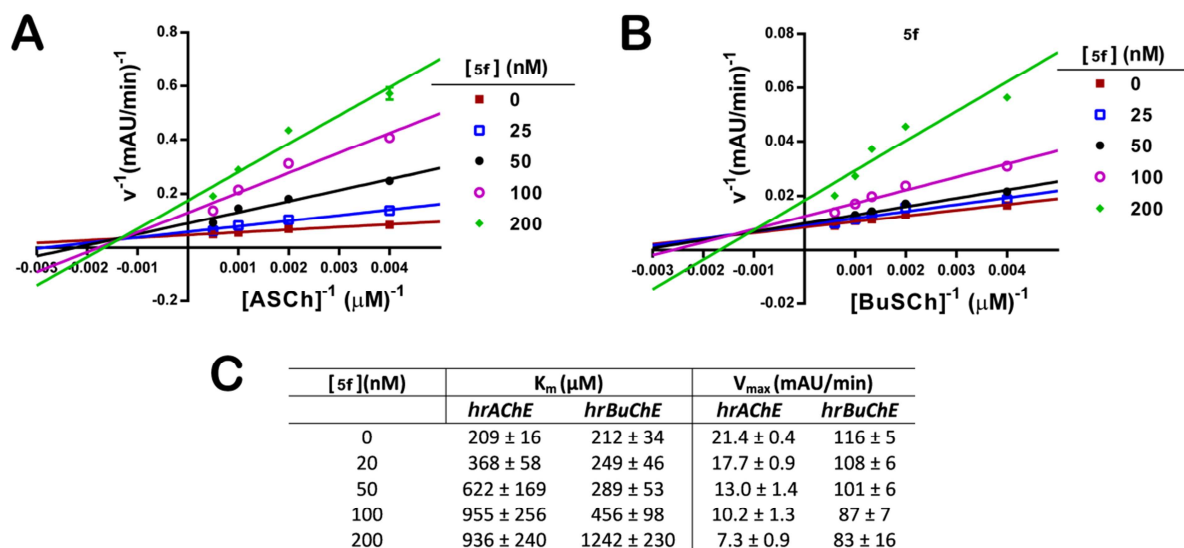
Figure 4. Kinetic assessment of **5f** as *hr*ChEs inhibitor. Lines were derived from a weighted least-squares analysis of data. Acetylthiocholine iodide (ASCh) and *S*-butyrylthiocholine iodide (BuSCh) were used as substrates.

For better characterizing compound **5f** inhibition properties at ChEs, kinetic assessments were performed as reported in Materials and Methods section. The results of this study are summarized in Figure 4. The assessment was performed by means of steady-state inhibition (Lineweaver-Burk plots of initial velocity) of *hr*AChE (Figure 4A) and *hr*BuChE (Figure 4B) by **5f** (0-200 nM) using acetylthiocholine iodide and *S*-butyrylthiocholine iodide (0.1-2 mM) as substrates, respectively. The data obtained by kinetic studies clearly showed a mixed-type inhibition for both enzymes since decreasing K_m values and increasing V_{max} values were determined as higher **5f** concentrations were used (Figure 4C). Moreover, non-linear analyses allowed to calculate inhibition constants (Ki) for **5f** inhibiting *hr*ChEs, and values of 14.9 ± 4.4 nM and 52.5 ± 16.6 nM were determined for *hr*AChE and *hr*BuChE, respectively.

13

2.2.2. Structure-activity relationship and molecular modeling studies

Computational studies allowed us to rationally explain the experimentally determined different selectivity degrees of compounds **5a-f** on the *hr*MAO-A and -B enzyme isoforms. The structural requirements governing the inhibitory potency of the title compounds on *hr*AChE were also investigated exploiting our experience in the field [29, 30, 40]. The potential binding modes of a subset of the analyzed compounds were found by applying the Induced Fit Docking (IFD) protocol [41] available in Schrödinger Suite [42] as already reported by us [31, 32]. The mentioned protocol involves various steps such as ligands and proteins preparation and molecular docking. In particular, in order to improve the reliability of our calculations, the ligands were prepared taking into account their protonation state at physiological pH (7.4) [33, 43-46]. In agreement with the literature data and software output, we have considered the 8-hydroxyquinoline moiety in its zwitterionic form, and the piperidine nitrogen as protonated (Table S1). Analysis of the data suggested that the presence of a CN group is relevant for improving MAO-A activity and selectivity (**5d** vs **5a**, **5e** vs **5b**, and **5f** vs **5c**, Table 1). For verifying this issue we have performed docking calculations for **5f** and **5c** in complex with *h*MAO enzymes. Results are depicted in Figure 5 for **5f** *S*-enantiomer (docking calculations of *R*-enantiomer were provided in Supporting Information in Figure S1) and in Figure 6 for **5c**. As shown in Figure 5A, compound (*S*)-**5f** interacts in the active site of MAO-A with a combination of polar contacts and hydrophobic interactions, targeting the key residues of the protein [47]. In particular, (*S*)-**5f** establishes a series of H-bonds with Lys305, Tyr444 and Phe208 (backbone), and a π-π stacking with Phe208 and with Phe352 (Figure 5A). In line with the experimentally determined irreversible mode of inhibition of **5f** (Figure 3), the propargylamine moiety of (*S*)-**5f** was found to lay in close proximity to the FAD molecule (3.3 Å). Accordingly, (*S*)-**5f** showed satisfactory docking score and free binding energy values (GlideXP score -10.82 kcal/mol, and ΔG_{bind} = -180.03 kcal/mol, respectively) which is consistent with good affinity for the isoform A of MAO enzyme. Notably, we observed a partial

14

stereoselective interaction with the enzyme. The *R*-enantiomer (Figure S1A) showed indeed a different pattern of interaction with respect to those found for the *S*-enantiomer. Although free binding energy values (GlideXP score and ΔG_{bind} of -8.54 kcal/mol and -176.16 kcal/mol) were found less favorable with respect to those obtained for the *S*-enantiomer, the different binding mode of (*R*)-**5f** with MAO-A, could prevent strong interactions with the enzyme. In fact, (*R*)-**5f** can establish only a π-π stacking with Phe173 and polar contacts with Val210 and Thr336. However, the propargylamine moiety lies far from the FAD molecule (14.1 Å) thus precluding a potential covalent interaction with the enzyme. These findings are in agreement with the micromolar inhibition potency found for the racemic mixture (the *S*-enantiomer showed an excellent predicted affinity with a binding mode that could allow a correct interaction within the enzyme, while the *R*-enantiomer appeared to possess a reduced predicted affinity).
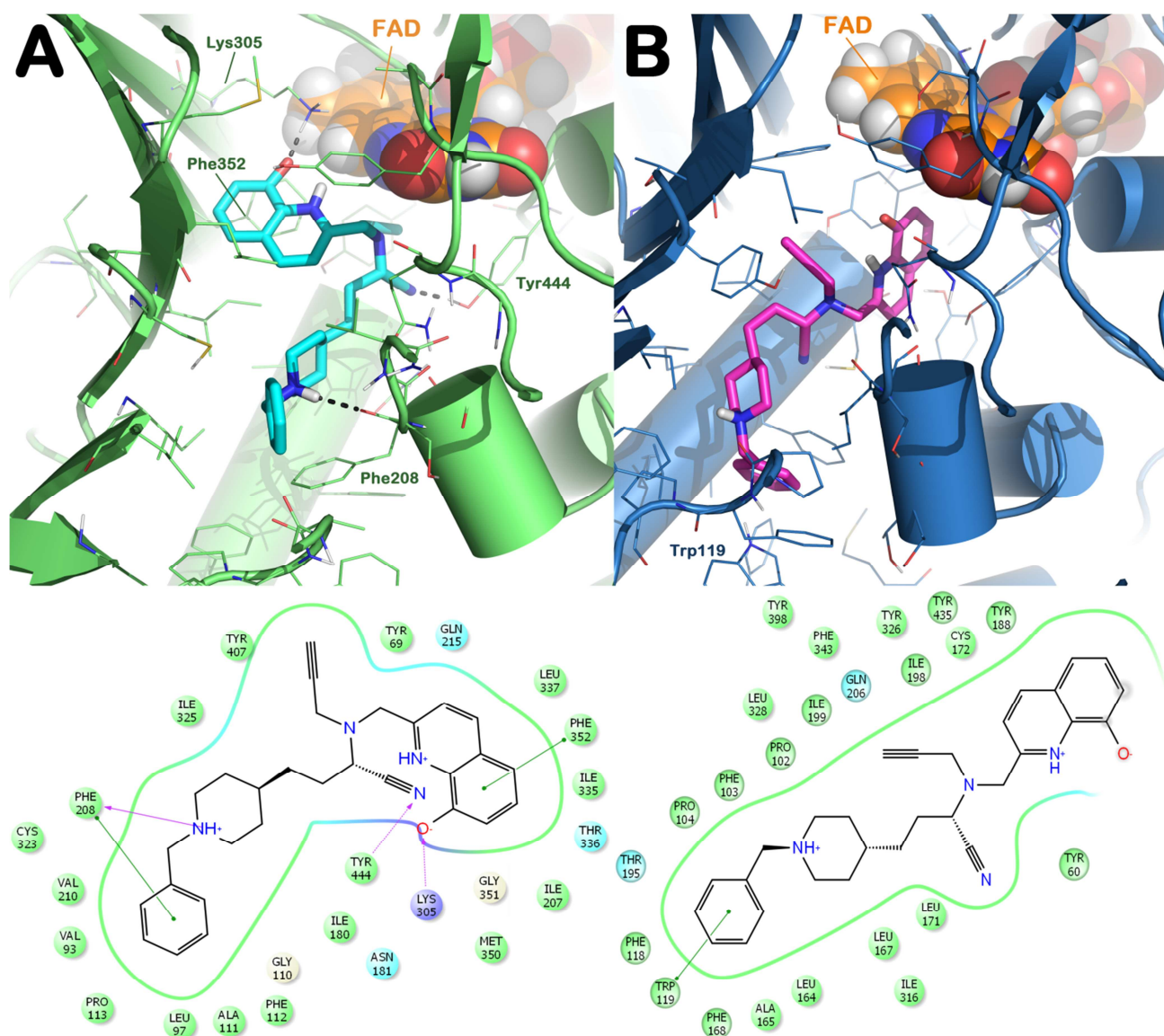
Figure 5. Docked pose of (*S*)-**5f** into *h*MAO-A (PDB ID: 2Z5X) (panel A) binding site and into *h*MAO-B (PDB ID: 2V5Z) (panel B). In the bottom part of the picture is represented a schematic ligand-protein interaction. The docked poses are visualized by means of PyMOL (The PyMOL Molecular Graphics System, v1.6-alpha; Schrodinger LLC, New York, NY, 2013), while the ligand-protein interaction diagram was generated by means of Maestro.

On the contrary, the IFD results obtained for (*S*)-**5f** revealed a poor affinity for MAO-B as depicted in

Figure 5B. Due to the different arrangement of the enzyme active sites, (*S*)-**5f** could not engage a

suitable pattern of interaction with the MAO-B binding site. In particular, the replacement of Ile335

and Ile180 (MAO-A) with Tyr326 and Leu171 (MAO-B) respectively appeared to limit cavity accessibility for our inhibitors. In addition, the replacement of Phe208 (MAO-A) with Ile199 (MAO-B) did not assure a correct accommodation of (*S*)-**5f** into MAO-B active site (Figure 5B). Consequently, the compound produced only a stacking with Trp119 that is located at the boundary of the binding pocket and no other contacts along the cleft were evident (Figure 5B). Moreover, the 8-hydroxyquinoline moiety appeared to be solvent exposed and the distance between the propargylamine and FAD is very large (8.74 Å) and not consistent with any potential covalent interaction. All these data and free binding energy calculation (GlideXP score -7.62 kcal/mol, and ΔG_{bind} is -127.49 kcal/mol) are in line with the observed MAO-A and -B selectivity. For, the (*R*)-**5f** (Figure S1B) we obtained similar results and no stereoselective interactions with MAO-B were detected (GlideXP score -8.04 kcal/mol and the ΔG_{bind} -130.81 kcal/mol). Similarly to the *S*-enantiomer into MAO-B with the *R*-enantiomer the distance of the propargylamine group from FAD (6.7 Å) did not assure any chance of covalent interaction thus well explaining the selectivity profile of **5f** for the two MAO isoforms.

For evaluating the influence of structural differences in MAO-A inhibition we have performed IFD studies also for **5c** for comparison with data obtained for **5f**. Compound **5c**, lacking the CN group, showed a decreased MAO-A inhibition activity when compared to **5f**, and the molecular docking output (Figure 6A) evidenced a slight different pattern of interaction with respect to **5f**. Indeed, **5c** could reproduce contacts with Lys305 and Phe208 (H-bonds), and could establish a π-π stacking with Phe352, but the absence of the CN group did not allow interaction with Tyr444 and the π-π stacking with Phe208 as for **5f** (Figure 6A). Moreover, the propargylamine group was found at 4.4 Å distance from the FAD molecule a larger distance than that found for **5f** (3.3 Å). All these evidences clearly demonstrate that the presence of the CN group is relevant for a better interaction with MAO-A binding site (**5c** indeed showed a slight decrease of docking score value and estimated free binding energy with respect to **5f**) and for higher inhibition potency (Table 1).

17
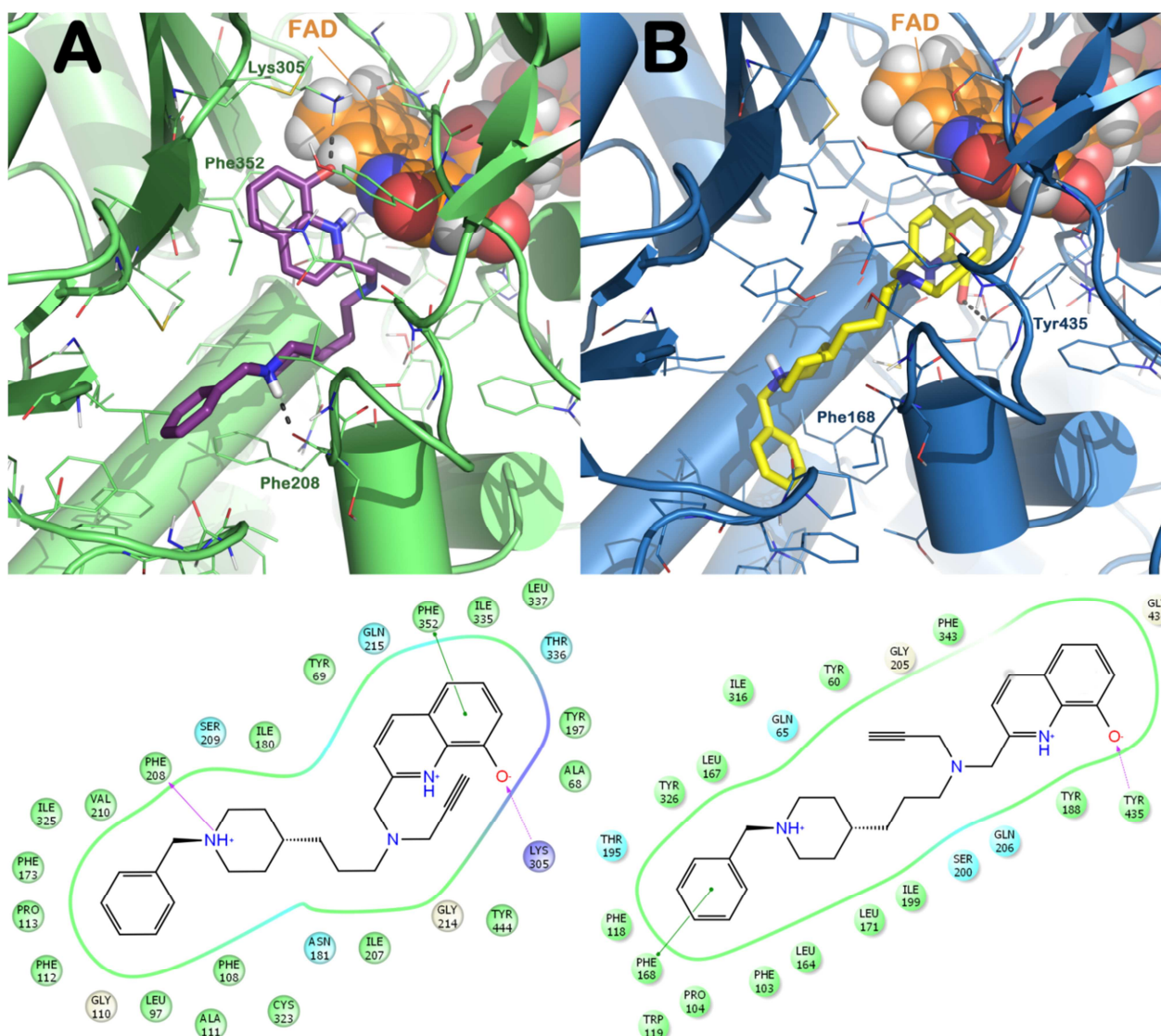
Figure 6. Docked pose of **5c** into *h*MAO-A (PDB ID: 2Z5X) (panel A; Docking score -9.96 kcal/mol; ΔG_{bind} = -174.29 kcal/mol) binding site and into *h*MAO-B (PDB ID: 2V5Z) (panel B; Docking score - 7.56 kcal/mol; ΔG_{bind} = -131.68 kcal/mol). In the bottom part of the picture is represented a schematic ligand-protein interaction.

Similarly to **5f**, also **5c** showed a poor MAO-B inhibition potency. Our docking results (Figure 6B) showed that **5c** is able to form only a H-bond with Tyr435 and a π-π stacking with Phe168 in a similar fashion to **5f**. Since the stacking with aromatic residues located at the boundary of the MAO-B binding site prevented a deep accommodation of the compound into the cleft, precluding strong interactions of

5c within the active site, the propargylamine group was found at 5.8 Å from FAD. All together these features led to a decrease of docking score values and of the estimated binding affinity in line with the poor MAO-B inhibition potency of **5c** (Table 1).

Overall this series of compounds (**5a-f**) was found to inhibit the *hr*ChEs from the micromolar to the nanomolar range and the compounds were in general more potent inhibitors of *hr*BuChE than *hr*AChE. Analysis of the data reported in Table 1 evidenced that *hr*AChE inhibition potency of the compounds is more sensible to small variations of the structure with respect to *hr*BuChE inhibition potency and this is in line with the wider gorge dimensions of the BuChE enzyme.

In order to better explain this behavior we performed IFD calculations for all the compounds within *h*AChE (PDB ID:1B41). The results (Figures 7 and 8) highlighted the importance of the length of the molecule for correct interaction with the enzyme since potency increased with the length of the compounds in both the **5a**-**c** and the CN containing **5d**-**f** sub-series. The lengthiest compounds **5c** and **5f** were indeed found to be the most potent *hr*AChE inhibitors of the series since they possess the correct distance between the aromatic moieties and an appropriately positioned basic center for interacting with the peripheral anionic site (PAS), mid-gorge, and catalytic site (CAS). In addition, the length of **5f** (*S*- and *R*-enantiomer) also assured a better accommodation of the CN group into the gorge of the enzyme with respect to the **5d** and **5e** (Figure 8 and Figure S2).
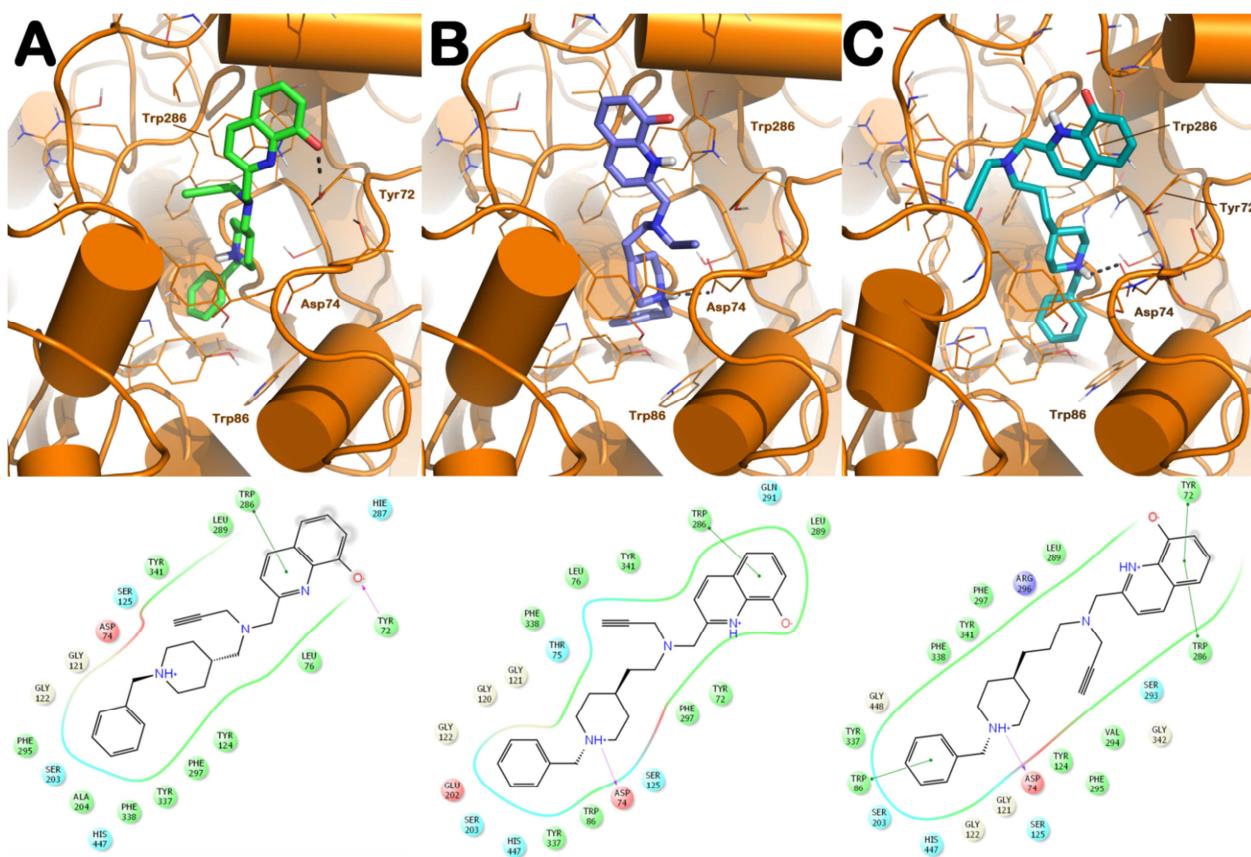
Figure 7. Docked poses of selected compounds (panels A-C; A: **5a**; B: **5b**; C: **5c**) into *h*AChE enzyme (PDB ID: 1B41). The pictures were generated by means of PyMOL, while the ligand-interaction diagrams were generated by means of Maestro.

In particular, the obtained binding mode of compound **5a** (Figure 7A) clearly revealed its impossibility to reach the CAS of *h*AChE. In fact, **5a** established a series of limited hydrophobic and polar contacts only with the PAS (Trp286 and Tyr72). Accordingly, the docking score and the ΔG_{bind} of **5a** are -7.91 kcal/mol and -84.26 kcal/mol, respectively. A moderate improvement in the inhibitory activity was observed with the homologation of linker between the propargylamine moiety and piperidine group. In fact, compound **5b** displayed a better accommodation into the binding site of *h*AChE (Figure 7B), interacting by a π-π stacking with Trp286 the PAS region with its 8-hydroxyquinoline moiety, and can engage a polar contact with the mid-gorge Asp74. These interactions account for the docking score and

the ΔG_{bind} of -8.91 kcal/mol and -102.22 kcal/mol, respectively. A further homologation was beneficial for activity and **5c** strongly interacted with PAS, mid-gorge and CAS recognition sites (Figure 7C). In particular, **5c** established a double π-π stacking with Trp286 and Tyr72 in the PAS and a polar contact with the mid-gorge region targeting the key residue Asp74. Notably, **5c** was also able to interact with the CAS by a π-π stacking with Trp86 by its benzyl moiety (Figure 7C). Also the docking score (-9.95 kcal/mol) and the ΔG_{bind} (-112.08 kcal/mol) supported the observed improvement of affinity of **5c** vs **5a** for *hr*AChE.

The same trend was observed with the introduction of CN group on the molecules **5d-f** (Figure 8). In fact, **5f** displayed the correct length and spatial arrangements of its features for appropriate interaction with *h*AChE. In fact, the CN group is perfectly tolerated in **5e** and **5f** establishing a series of relevant polar interactions with Phe295 or/and Arg296 (backbone) as reported in Figure 8B,C and in Figure S2, accounting for the favorable docking score and ΔG_{bind}. Notably, and in line with the IC_{50} values (Table 1), our computational analysis also revealed that the mid-gorge Asp74 is targeted by both enantiomers of **5f** and by only one enantiomer of **5e**.

21
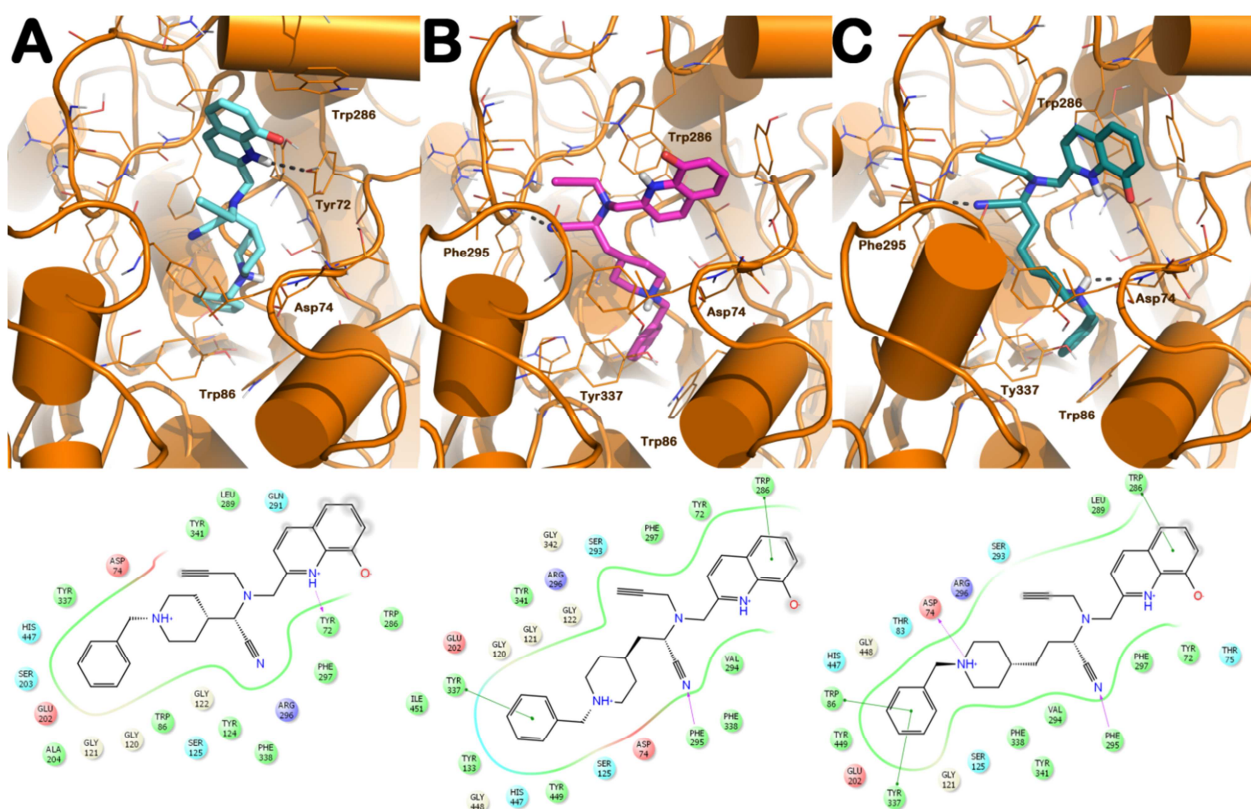
Figure 7. Docked poses of *S*-enantiomer of selected compounds (A-C; A: **5d**; B: **5e**; C: **5f**) into *h*AChE enzyme (PDB ID: 1B41). The docking output for the *R*-enantiomers is provided in Figure S2. The pictures were generated by means of PyMOL, while the ligand-interaction diagrams were generated by means of Maestro.

Our calculations also explained the worst *hr*AChE inhibition properties of **5d** (*S*- and *R*-enantiomer) which did not establish interactions at the mid-gorge and CAS level as observed for the analogue **5a** devoid of the CN group. **5d** only interacts with PAS by a H-bond with Tyr72 by its 8-hydroxyquinoline moiety (Figure 8A and Figure S2A). Notably, a non-classical conformation of Trp286 was detected which supported the poorest affinity of **5d** for *hr*AChE. Also the docking score values (*S*-enantiomer -7.58 kcal/mol; *R*-enantiomer -7.33 kcal/mol) and ΔG_{bind} (*S*-enantiomer -79.42 kcal/mol; *R*-enantiomer -78.15 kcal/mol) are in agreement with a 6-fold lower potency with respect to **5a**. As above reported for compound **5b**, the elongation of the spacer in this scaffold improved *hr*AChE inhibition potency. In

fact, **5e** (*S*- and *R*-enantiomer, Figure 8B and Figure S2B, respectively) inhibiting *hr*AChE in the micromolar range revealed a better pattern of interaction than **5d**. In fact, **5e** established a series of contacts with PAS and mid-gorge, but could not reach the CAS due to the lack of appropriate length of the linker. In particular (*S*)-**5e** established a π-π stacking by its aromatic moieties with Trp286 and with Tyr337 (Figure 8B). In addition, the CN group interacts with the backbone of Phe295 by a H-bond. The improvement of affinity by one order of magnitude was confirmed by the presence of a stronger pattern of interaction with *h*AChE and a satisfactory docking score (-9.46 kcal/mol) coupled to a significant ΔG_{bind} of -109.81 kcal/mol. In addition, the *R*-enantiomer lacks the interaction with Tyr337 but it forms a H-bond with the mid-gorge site Asp74 (Figure S2B). A comparable docking score (-10.34 kcal/mol) and ΔG_{bind} (-107.60 kcal/mol) were found for the *R*-enantiomer with respect to the *S*-enantiomer.

Finally, the IFD calculation performed on **5f**, possessing the appropriate length for optimally targeting all the key interaction sites of *h*AChE gorge (Figures 8C and S2C), revealed a good fitting within the enzyme. In particular, (*S*)-**5f** was able to establish a double π-π stacking by its 8-hydroxyquinoline and benzyl groups with Trp286 and Trp86/Tyr337, respectively. Moreover, a series of H-bonds were found with Phe295 by the CN group, and with Asp74 by the piperidine moiety. This enantiomer showed a very high docking score (-12.93 kcal/mol) as well as the estimated free-binding energy (ΔG_{bind} -129.67 kcal/mol). Similarly, the *R*-enantiomer (Figure S2C) was able to reproduce all the contacts found for the *S*-enantiomer (Figure 8C) with few additional contacts (H-bonds with the backbone of Arg296 by its CN group, with Tyr72 sidechain by its 8-hydroxyquinoline moiety, and a π-π stacking with His447 by the benzyl moiety, Figure S2C). These additional contacts led to a significant improvement in the docking score (-14.87 kcal/mol) as well as in the ΔG_{bind} (-146.31 kcal/mol). This strong pattern of interaction found for both **5f** enantiomers perfectly parallels and explains the *in vitro* data (Table 1).

Last, but not least, all the compounds showed an excellent drug-like profile (ADME+T properties prediction) as calculated by means of QikProp [48] (Table 2).

Table 2. Calculated physicochemical properties for compounds presented in this study by means of QikProp application.

Cpd	SASA[a]	QPlogP[b]	QPlogS[c]	QPlogHERG[d]	%HOA[e]
5a	743.9	3.78	-3.37	-8.21	88.0
5b	800.9	4.84	-4.59	-8.90	95.4
5c	827.7	5.19	-4.91	-8.89	84.7
5d	757.1	3.03	-3.80	-8.23	75.2
5e	818.1	4.23	-5.18	-8.87	84.6
5f	851.7	4.50	-5.61	-8.97	84.2

The calculated properties and their recommended range according to QikProp user manual are follows: [a]SASA 300-1000; [b]QPlogP -2.00 – 6.5; [c]QPlogS -6.5 – 0.5; [d]QPlogHERG <-5; [e]%HOA: %human oral absorption >80% high, <25% poor.

2.2.3. Assessment of metal-chelating properties of 5f

Our investigation of the relevant properties of compound **5f** as a potential DMAAD was implemented with the *in vitro* assay for establishing its metal-chelating properties. Chelating tests reported in Figure 9 allowed to understand the metal-chelating properties of **5f** evaluating the formation of metal-complexes. Indeed, the ability of **5f** to interact with metals relevant for Aβ misfolding such as zinc, copper, and iron was assessed [49].

24
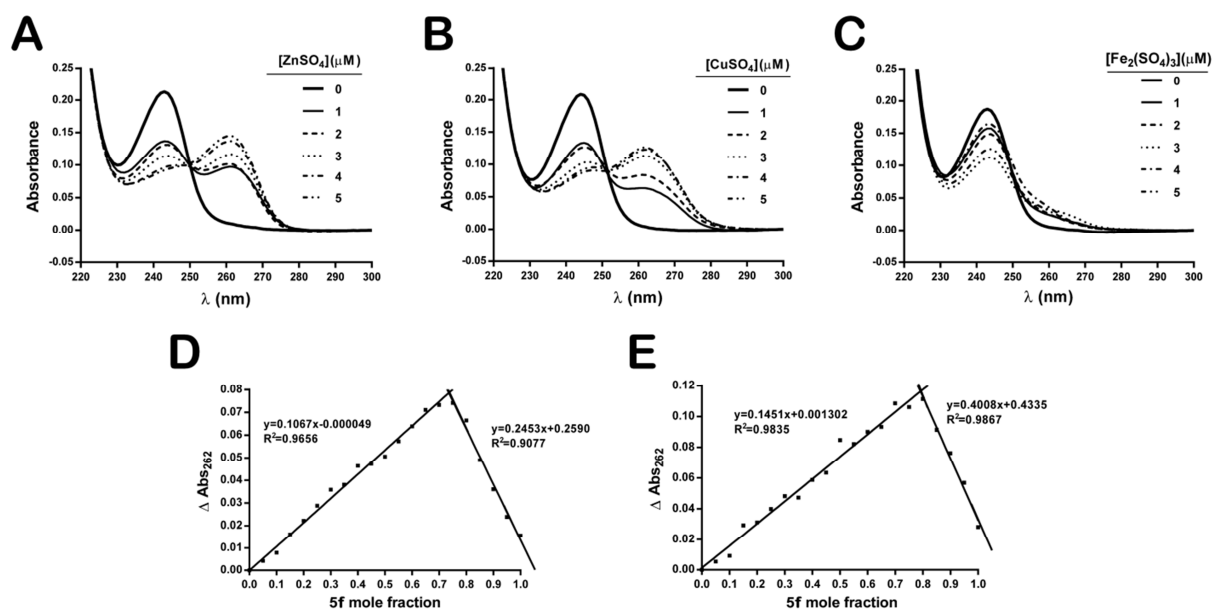
Figure 9. Assessment of metal-chelating properties of compound **5f**. UV-VIS spectra of solutions containing 10 μM **5f** shortly incubated with increasing concentrations (0-5 μM) of metals $ZnSO_4$ (A), $CuSO_4$ (B) and $Fe_2(SO_4)_3$ (C). Determination of the stoichiometry of complexes **5f**-Zn(II) (D) and **5f**-Cu(II) (E) by using the Job's method at 262 nm. All solutions were prepared in still water and experiments were performed at room temperature.

In particular, the influence of abnormally high levels of redox-active metal ions such as Cu^{2+}, Fe^{2+} was characterized as well as the compromised regulation of redox-active metals in the promotion and formation of cytotoxic ROS and neuronal damage [50]. Moreover, the role of mentioned metals in formation and progression of aberrant Aβ species causing the misfolding of proteins and their subsequent aggregation was also established. Numerous studies have demonstrated that a surplus of metal ions such as Cu^{2+}, Fe^{2+}, Zn^{2+} and Al^{3+} were present in Aβ plaques of AD patients' brain [49]. Furthermore an excess of Cu^{2+} and Zn^{2+} promotes Aβ aggregation [51, 52]. For these reasons, the research with multitarget compounds additionally decorated for obtaining metal-chelating effect might provide an additional and therapeutic, rather than only symptomatological, strategy for the treatment of AD. Our *in vitro* analyses (Figure 9) reveal that **5f** is able to interact with metals. Additionally, an extinction coefficient (ε) of 20800 $M^{-1} \cdot cm^{-1}$ was determined with **5f**, while a maximum complexation

peak was detected at 262 nm. As showed in Figure 9A, **5f** displayed a spectral changes at 10 μM forming a complex with Zn^{2+} after incubations of 15 h. Remarkably, **5f** formed a complex with Cu^{2+} (Figure 9B) after 5 minutes of incubation. On the contrary, with Fe^{3+} (Figure 9C) no significant spectral changes were observed at 262 nm after longer pre-incubations. In summary, **5f** was determined as metal-chelating agent, a stoichiometry complexation of 1:2 metal-compound with both Cu^{2+} (Figure 9D) and Zn^{2+} (Figure 9E) revealed a metal-compound ration of 1:2.

2.2.4. Evaluation of antioxidant properties of 5f

The assessment of antioxidant properties of compound **5f** was carried out by different *in vitro* assays. Figure 10A shows the Cu(II)-chelating activity of **5f** at blocking the production of H_2O_2 *in vitro* by Cu(II) and ascorbic acid using the Amplex Red reagent. This effect was in agreement with the metal-chelating properties previously observed as a stoichiometry of 1:2 Cu(II)/compound was also found. Compound **5f** also displayed oxygen radical absorbance capacity (ORAC) values equivalent to those observed with the antioxidant Trolox (Figure 10B). Lipid peroxidation induced *in vitro* by linoleic acid and 2,2'-azobis(2-amidinopropane) dihydrochloride (AAPH) (Figure 10C) was significantly reduced by **5f** though this effect was prolonged similarly (T_{inh}) over time as that observed in the control. Finally, compound **5f** was shown to induce weak radical scavenger activity (RSA) compared to trolox by using 2,2-difenil-1-picrilidrazile (**DPPH**, Figure 10D). Although a dose-dependent effect was found with **5f**, being significant from concentrations higher than 50 μM, no similar antioxidant response was reached compared to that of 50 μM trolox at any of the concentrations assayed with **5f**.
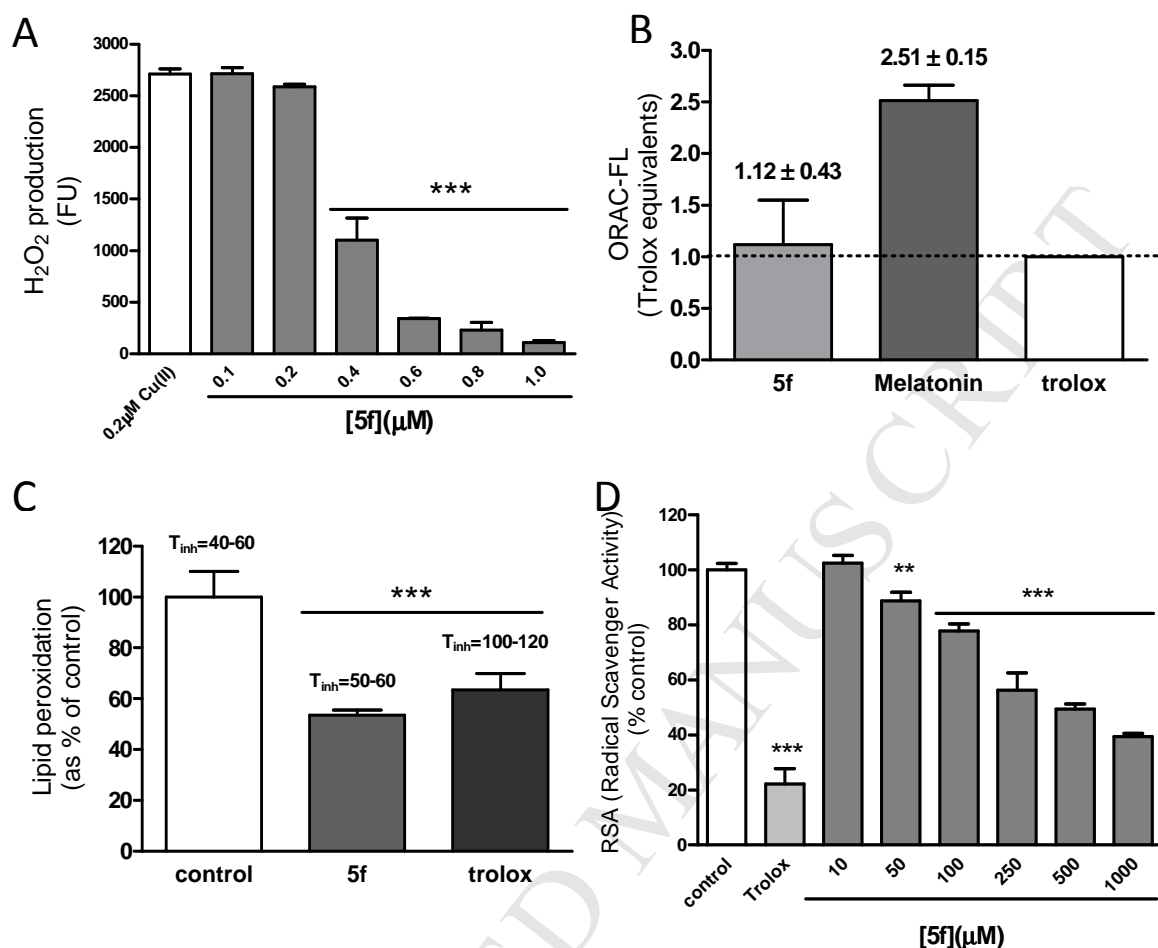
Figure 10. Evaluation of *in vitro* antioxidant properties of compound **5f**.
A) Effect of compound **5f** on the *in vitro* production of H_2O_2 in presence of Cu(II) and ascorbic acid expressed in fluorescence units (FU); B) ORAC-FL values of **5f** and melatonin as trolox equivalents; C) inhibition of lipid peroxidation (LPO) by compound **5f** and trolox (inhibition times (T_{inh}) are expressed in min); D) radical scavenger activity (RSA) induced by DPPH with compound **5f** and 50 μM trolox. Statistical analysis was performed using one-way ANOVA test followed by Bonferroni post-test. **, $p<0.01$, ***, $p<0.001$.

3. Conclusion

In summary, in this study, the development of novel donepezil-related compounds (**5a-f**) characterized by a multifunctional profile is reported. Among the series of the novel chemical entities assayed, compound **5f** exhibited the most interesting profile to be further characterized as AD potential therapeutic. In fact, **5f** was defined as a mixed-type *hr*AChE and *hr*BuChE inhibitor of nanomolar

potency, and was also found a selective irreversible MAO-A inhibitor in the micromolar range. Molecular modeling studies were performed to rationalize the mode of action and the selectivity profile of the developed compounds. These studies evidenced the structural requirements of these donepezil-related analogues to optimally interact with the enzymes of interest. Additionally, **5f**, conceived for interacting with metals targeting the cytotoxicity derived from Aβ misfolding leading to oligomers formation, was demonstrated to be able to form complexes with Zn^{2+} and Cu^{2+}. These data confirm **5f** metal-chelating properties which might be relevant for modulating Aβ misfolding. Furthermore, **5f** is also endowed with some antioxidant properties. The calculated physico-chemical properties enrich the profile of this promising hit as it shows a drug-likeness in line with other marketed drugs. Taken together these findings will pave the way to the development of novel anti-AD based on **5f** that deserves to be further investigated as DMAAD.

4. Experimental section

4.1. Chemistry

4.1.1. General procedures

Unless otherwise specified, materials were purchased from commercial suppliers and used without further purification. Silica gel 60 (0.040 - 0.063 mm) were used for column chromatography. ^{1}H NMR, and ^{13}C NMR, spectra were recorded on a Varian INOVA-600, Varian INOVA-400 or Varian Mercury 300MHz, spectrometers by using the residual signal of the deuterated solvent as internal standard. Splitting patterns are described as singlet (s), doublet (d), triplet (t), quartet (q), quintet (p), and broad (br); the value of chemical shifts (d) are given in ppm and coupling constants (*J*) in Hertz (Hz). IR spectra were obtained with a Shimazu, Model FT-IR 8400. Purity of the compounds was assessed by

HRMS, spectra were recorded on a Bruker Daltonics Bio TOF mass spectrometer. Yields refer to purified products and are not optimized. All moisture-sensitive reactions were performed under argon atmosphere using oven-dried glassware and anhydrous solvents.

4.1.2. 2-(1-Benzylpiperidin-4-ylidene)acetonitrile (8a)

Diethyl (cyanomethyl)phosphonate (7). Chloroacetonitrile (3 g, 40 mmol) and triethyl phosphite (6.65 g, 40 mmol) were heated at 150 ^{o}C for 3.5 h. And the crude product was directly used in the next reactions.

A solution of diethyl (cyanomethyl)phosphonate **7** (2.13 g, 12 mmol) and K_2CO_3 (1.66 g, 12 mmol) in 10 mL of dry THF was stirred for 15 min at rt. Then the mixture was heated to reflux for 20 min. After cooling down to rt, ketone **6a** (10 mmol of in 5 mL of dry THF) was added dropwise to this mixture and then resulting mixture was heated at reflux for 12 h. After cooling down to rt, 10% K_2CO_3 aqueous solution was added. The reaction mixture was extracted with AcOEt three times, the organic phase were collected, dried with anhydrous Na_2SO_4 and concentrated in vacuum to obtain the crude product which was directly used for the following reactions without further purification. Title compound was obtained as yellow oil, 92.0% yield; ^{1}H NMR (300 MHz, CDCl$_3$) δ 7.26–7.34 (m, 5 H), 5.10 (s, 1 H), 3.55 (s, 2 H), 2.51–2.63 (m, 6 H), 2.40 (t, *J* = 5.1 Hz, 2 H).

4.1.3. 3-(1-Benzylpiperidin-4-yl)acrylonitrile (8b).

Following the procedure described for compound **8a** the title compound was obtained as yellow oil, 95.0% yield; ^{1}H NMR (300 MHz, CDCl$_3$) δ7.19–7.38 (m, 5 H), 6.31 (t, *J* = 10.4 Hz, 1 H), 5.23 (d, *J* = 10.9 Hz, 1 H), 3.50 (s, 2 H), 2.89 (d, *J* = 11.7 Hz, 2 H), 2.51–2.71 (m, 1 H), 1.93–2.14 (m, 2 H), 1.62–1.77 (m, 2 H), 1.40–1.60 (m, 2 H).

4.1.4. 2-(1-Benzylpiperidin-4-yl)acetonitrile (9a).

To a solution of compound **8a** (7.7 mmol) in 35 mL MeOH, Mg (154 mmol) and catalytic amount of I_2 were added while stirring at rt. The mixture was then stirred in an ice bath was until the reaction mixture became gray gel. Then, conc. HCl was slowly added till the reaction became clear. 10 N NaOH was added to neutralize the pH to 8-9. The precipitate was filtered and washed with large amount of AcOEt. The filtrate was extracted with AcOEt three times, and the combined organic layers were dried with anhydrous Na_2SO_4 and concentrated in vacuum to give the crude product which was directly used for the following reactions without further purification. Title compound was obtained as yellow oil 82% yield; ^{1}H NMR (300 MHz, CDCl$_3$) δ 7.24–7.34 (m, 5 H), 3.55 (s, 2 H), 2.93 (d, *J* = 11.8 Hz, 2 H), 2.28 (d, *J* = 6.60 Hz, 2 H), 2.00 (t, *J* = 52.77 Hz, 2 H), 1.78 (m, 2 H), 1.68 (m, 1 H), 1.48 (m, 2 H).

*4.1.5. 3-(1-Benzylpiperidin-4-yl)propanenitrile (**9b**).*

Following the procedure described for compound **9a** the title compound was obtained as yellow oil 87% yield; ^{1}H NMR (300 MHz, CDCl$_3$) δ 7.19–7.37 (m, 5 H), 3.50 (s, 2 H), 2.89 (d, *J* = 11.8 Hz, 2 H), 2.35 (t, *J* = 7.3 Hz, 2 H), 1.96 (td, *J* = 11.5, 1.9 Hz, 2 H), 1.54–1.73 (m, 4 H), 1.17–1.52 (m, 3 H).

*4.1.6. 2-(1-Benzylpiperidin-4-yl)acetaldehyde (**10a**).*

An over dried and argon-purged flask nitrile **9a** (10.0 mmol) in 20 mL of dry toluene was cooled to –78 ^{o}C, and 12 mL 1 mol/L DIBAL-H toluene solution was added dropwise to the solution. The reaction mixture was stirred at –78 ^{o}C for 1.5 h. Then 10 mL MeOH were added, and the solution was poured into 100 mL 5% H_2SO_4 aqueous solution and then alkaline with conc. NH$_4$OH. The precipitate was filtered and washed with AcOEt. The filtrate was extracted with AcOEt for three times. The combined organic phase was washed with brine and dried with anhydrous Na_2SO_4. After concentration, the crude product was purified by silica gel chromatography Hex/AcOEt, 2:1 to give pure title compound as orange oil, 87% yield; ^{1}H NMR (300 MHz, CDCl$_3$) δ 9.76 (t, *J* = 1.9 Hz, 1 H), 7.17–7.42 (m, 5 H),

3.51 (s, 2 H), 2.88 (d, J = 11.2 Hz, 2 H), 2.36 (dd, J = 6.7, 1.76 Hz, 2 H), 1.60–2.15 (m, 5 H), 1.20–1.50 (m, 2 H).

*4.1.7. 3-(1-Benzylpiperidin-4-yl)propanal (**10b**).*

Following the procedure described for compound **10a** the title compound was obtained as yellow oil, 83% yield; ^{1}H NMR (400 MHz, CDCl$_3$) δ 9.76 (t, J = 1.6 Hz, 1 H), 7.19–7.38 (m, 5 H), 3.44–3.53 (m, 2 H), 2.87 (d, J = 11.1 Hz, 2 H), 2.43 (td, J = 7.5, 1.6 Hz, 2 H), 1.92 (t, J = 11.8 Hz, 2 H), 1.52–1.72 (m, 4 H), 1.16–1.35 (m, 3 H).

*4.1.8. 8-Hydroxyquinoline-2-carbaldehyde (**12**).*

SeO$_2$ (20 mmol, 2.22 g) in 70 mL 1.4-dioxane and 1 mL water mixture were heated to 60 $^{\circ}$C. To this solution 2-methylquinolin-8-ol **11** (1.59 g, 10 mmol) in 15 mL 1.4-dioxane was added dropwise over 30 min. The obtained mixture was heated at reflux for 12 h. After cooling down to rt, the precipitate was filtered and the filtrate was concentrated. The crude product was purified by silica gel chromatography using Hex/AcOEt, 5:1 to give 1.49 g of pure title compound as yellow solid, 86% yield; ^{1}H NMR (600 MHz, CDCl$_3$), δ 10.22 (s, 1H), 8.32 (d, J = 8.4 Hz, 1H), 8.20 (br, 1H), 8.06 (d, J = 8.4 Hz, 1H), 7.62 (t, J = 7.8 Hz, 1H), 7.43 (d, J = 8.4 Hz, 5H), 7.29-7.26(m, 1H), 7.16 (d, J = 7.2 Hz, 1H).

*4.1.9. 8-((tert-Butyldimethylsilyl)oxy)quinoline-2-carbaldehyde (**13**).*

To a solution of **12** (1.5 g, 8.66 mmol) and imidazole (1.3 g, 19.1 mmol) in 30 mL of dry DCM *tert*-butylchlorodimethylsilane (1.44 g, 9.53 mmol) was added while stirring at 0 $^{\circ}$C. The mixture was allowed to warm slowly to rt for further 16 h while stirring, then 30 mL water were added. The aqueous phase was extracted with DCM three times and the combined organic phase was washed with saturated NaHCO$_3$ solution, brine and dried with anhydrous Na$_2$SO$_4$. After concentration in vacuum, the crude

product was purified by silica gel chromatography using Hex/AcOEt, 10:1 to give 2.16 g of pure title compound as yellow oil, 87% yield, ^{1}H NMR (600 MHz, CDCl$_3$), δ 10.22 (d, J = 0.6 Hz, 1H), 8.25 (d, J = 8.4 Hz, 1H), 7.99 (d, J = 8.4 Hz, 1H), 7.56-7.54 (m, 1H), 7.48 (d, J = 8.4 Hz, 5H), 7.25-7.24 (m, 2H), 1.09 (s, 9H), 0.32 (s, 6H).

*4.1.10. N-((8-((tert-Butyldimethylsilyl)oxy)quinolin-2-yl)methyl)prop-2-yn-1-amine (**14**).*

Aldehyde **13** (1.44 g, 5 mmol) and prop-2-yn-1-amine (550 mg, 10 mmol) were dissolved in 50 mL of MeOH and cooled to 0 ^{o}C. 10 drops of CF$_3$COOH were added and the reaction mixture was stirred at 0 ^{o}C for 1 h and rt for further 2 h. Then NaBH$_4$ (380 mg, 10 mmol) were added to the reaction at 0 ^{o}C and the obtained mixture was stirred for another 1 h at rt. The reaction was quenched with 50 mL of saturated NH$_4$Cl solution and the water phase was extracted with AcOEt for three times. The combinied organic phase was washed with brine and dried with anhydrous Na$_2$SO$_4$. After concentrated in vacuum, the crude product was purified by silica gel chromatography using a mixture Hex/AcOEt, 2:1 to give 1.4 g of pure title compound as yellow oil, 86% yield; ^{1}H NMR (600 MHz, CDCl$_3$), δ 8.07 (dd, J = 1.8 Hz, J = 8.4 Hz, 1H), 7.41-7.36 (m, 3H), 7.15-7.14 (m, 1H), 4.21 (d, J = 1.2 Hz, 2H), 3.58 (dd, J = 1.8 Hz, J = 2.4 Hz, 1H), 2.90 (br, 1H), 2.25 3.58 (d, J = 1.8 Hz, 1H), 1.08 (s, 9H), 0.25 (s, 6H).

*4.1.11.   N-((1-benzylpiperidin-4-yl)methyl)-N-((8-((tert-butyldimethylsilyl)oxy)quinolin-2-yl)methyl)prop-2-yn-1-amine (**15a**).*

A mixture of amine **14** and 1 mmol and aldehyde **6b** (1.5 mmol) in MeOH (10 mL) was cooled at 0 ^{o}C. 3 drops of CF$_3$COOH were added, and the reaction was stirred at 0 ^{o}C for 1 h and then kept at rt for 12 h. After that time NaBH$_4$ (3 mmol) was added at 0 ^{o}C and the reaction was stirred for 1 h at rt. 20 mL saturated NH$_4$Cl solution were then added to quench the reaction, and water phase was extracted with AcOEt for three times. The combined organic phase was washed with brine and dried with anhydrous Na$_2$SO$_4$. After concentration in vacuum, the crude product was purified by silica gel chromatography

using Hex/AcOEt from 10:1 to 2:1 to obtain the pure title compound as yellow oil, 54.6% yield. The title compound was submitted to the following step without any further characterization.

4.1.12. *N-(2-(1-benzylpiperidin-4-yl)ethyl)-N-((8-((tert-butyldimethylsilyl)oxy)quinolin-2-yl)methyl)prop-2-yn-1-amine (15b).*

Following the procedure described for compound **15a** the title compound was obtained as yellow oil, 51.2% yield. The title compound was submitted to the following step without any further characterization.

4.1.13. *N-(3-(1-benzylpiperidin-4-yl)propyl)-N-((8-((tert-butyldimethylsilyl)oxy)quinolin-2-yl)methyl)prop-2-yn-1-amine (15c).*

Following the procedure described for compound **15a** the title compound was obtained as yellow oil, 46.1% yield. The title compound was submitted to the following step without any further characterization.

4.1.14. 2-((((1-Benzylpiperidin-4-yl)methyl)(prop-2-yn-1-yl)amino)methyl)quinolin-8-ol (5a).

To a solution of **15a** (0.4 mmol) in 10 mL of THF a 2 mL of a 1 M solution of TBAF in THF were added and the mixture was stirred at rt for 3 h. Then the solvent was removed, and the residue was purified by silica gel chromatography using Hex/AcOEt from 10:1 to 1:1 to obtain the pure title compound as yellow oil, 93.5% yield IR ν_{max} = 3289, 2922, 2801, 1713, 1601, 1574, 1506, 1474, 1456, 1435, 1366, 1327, 1279, 1246, 1220, 1202, 1126, 1117, 1090, 1076, 984, 909, 833, 754, 739. ^{1}H NMR (400 MHz, CDCl$_3$), δ 8.08 (d, *J* = 8.4 Hz, 1H), 7.62 (d, *J* = 8.4 Hz, 1H), 7.41 (t, *J* = 7.8 Hz, 1H), 7.30-7.25 (m, 5H), 7.25-7.23(m, 1H), 7.16 (d, *J* = 7.2 Hz, 1H), 3.93(s, 2H), 3.48 (s 2H), 3.40 (s 2H), 2.87 (d, *J* = 10.8 Hz, 2H), 2.44 (d, *J* = 7.2 Hz, 2H), 2.26 (d, *J* = 1.8 Hz, 1H), 1.93 (t, *J* = 11.4 Hz, 2H), 1.77 (d, *J* = 12.6 Hz, 2H), 1.53-1.50 (m, 1H), 1.21-1.15 (m, 2H); ^{13}C NMR (150 MHz, CDCl$_3$), δ 158.1, 152.0,

138.5, 137.4, 136.4, 129.2, 128.1, 127.5, 127.2, 126.9, 121.8, 117.6, 110.0, 78.7, 73.3, 63.5, 60.7, 59.3, 53.6, 42.8, 33.7, 30.7. HRMS (ESI): m/z [M + H]$^+$ calcd for C$_{26}$H$_{30}$N$_3$O: 400.2383; found 400.2387.

*4.1.15. 2-(((2-(1-Benzylpiperidin-4-yl)ethyl)(prop-2-yn-1-yl)amino)methyl)quinolin-8-ol (**5b**).*

Following the procedure described for compound **5a** the title compound was obtained as yellow oil, 91.6% yield; IR ν$_{max}$ = 3302, 2911, 2797, 2787, 1713, 1574, 1506, 1474, 1454, 1435, 1396, 1366, 1327, 1248, 1200, 1150, 1123, 1086, 978, 910, 839, 754, 738. ^{1}H NMR (400 MHz, CDCl$_3$), δ 8.09(d, J = 8.4 Hz, 1H), 7.60 (d, J = 8.4 Hz, 1H), 7.40 (t, J = 7.8 Hz, 1H), 7.30-7.25 (m, 5H), 7.25-7.23 (m, 1H), 7.16 (d, J = 7.2 Hz, 1H), 3.94 (s, 2H), 3.47 (s, 2H), 3.41 (d, J = 2.4 Hz, 2H), 2.84 (d, J = 11.4 Hz, 2H), 2.62 (t, J = 7.2 Hz, 2H), 2.26 (d, J = 1.8 Hz, 1H), 1.90 (t, J = 12.0 Hz, 2H), 1.59 (d, J = 12.6 Hz, 2H), 1.46-1.44 (m, 2H), 1.31-1.25 (m, 3H); ^{13}C NMR (150 MHz, CDCl$_3$), δ 157.8, 152.1, 138.5, 137.5, 136.4, 129.2, 128.2, 127.5, 127.3, 126.9, 121.8, 117.6, 110.0, 78.5, 73.3, 63.5, 60.3, 53.8, 51.0, 42.4, 34.2, 33.8, 32.4, 31.6. HRMS (ESI): m/z [M + H]$^+$ calcd for C$_{27}$H$_{32}$N$_3$O: 414.2540; found 414.2539.

*4.1.16. 2-(((3-(1-Benzylpiperidin-4-yl)propyl)(prop-2-yn-1-yl)amino)methyl)quinolin-8-ol (**5c**).*

Following the procedure described for compound **5a** the title compound was obtained as yellow oil, 97.1% yield. IR ν$_{max}$ = 3300, 2907, 27847, 2797, 2758, 1713, 1601, 1574, 1506, 1471, 1454, 1435, 1368, 1327, 1248, 1200, 1125, 1090, 972, 910, 839, 735. ^{1}H NMR (400 MHz, CDCl$_3$), δ 8.08(d, J = 9.0 Hz, 1H), 7.60 (d, J = 8.4 Hz, 1H), 7.40 (t, J = 7.8 Hz, 1H), 7.30-7.28 (m, 5H), 7.25-7.22 (m, 1H), 7.16 (d, J = 7.8 Hz, 1H), 3.94 (s, 2H), 3.46 (s, 2H), 3.41 (d, J = 2.4 Hz, 2H), 2.84 (d, J = 11.4 Hz, 2H), 2.57 (t, J = 7.2 Hz, 2H), 2.25 (d, J = 1.2 Hz, 1H), 2.14 (s, 1H), 1.86 (t, J = 12.0 Hz, 2H), 1.60 (d, J = 12.0 Hz, 2H), 1.52-1.50 (m, 2H), 1.26-1.18 (m, 5H); ^{13}C NMR (150 MHz, CDCl$_3$), δ 157.8, 152.1, 138.5, 137.5, 136.4, 129.2, 128.1, 127.5, 127.2, 126.9, 121.9, 117.6, 110.0, 78.6, 73.3, 63.5, 60.2, 53.9, 53.6, 42.4, 35.5, 34.1, 32.4, 24.7. HRMS (ESI): m/z [M + H]$^+$ calcd for C$_{28}$H$_{34}$N$_3$O: 428.2696; found 428.2700.

4.1.17.   2-(1-Benzylpiperidin-4-yl)-2-(((8-(tert-butyldimethylsilyloxy)quinolin-2-yl)methyl)(prop-2-ynyl)amino)acetonitrile (17a).

To a mixture of aldehyde **6a** (1.5 mmol) and TMSCN (2 mmol in 20 mL DCM, ZnI$_2$ (0.2 mmol) was added, and the reaction mixture was stirred for 1 h at rt the intermediate compound **16a**. After removal of the solvent amine **14** (1 mmol) in MeOH (15 mL) was added and the resulting mixture was heated to 50 $^{\circ}$C for further 3 h. After that, MeOH was removed and the residue was purified by silica gel chromatography Hex/AcOEt from 10:1 to 2:1 to obtain pure title compounds as yellow oil 54% yield. The title compound was submitted to the following step without any further characterization.

4.1.18.   3-(1-Benzylpiperidin-4-yl)-2-(((8-(tert-butyldimethylsilyloxy)quinolin-2-yl)methyl)(prop-2-ynyl)amino)propanenitrile (17b).

Following the procedure described for compound **17a** the title compound was obtained as yellow oil, 31.8% yield. The title compound was submitted to the following step without any further characterization.

4.1.19.   4-(1-Benzylpiperidin-4-yl)-2-(((8-(tert-butyldimethylsilyloxy)quinolin-2-yl)methyl)(prop-2-ynyl)amino)butanenitrile (17c).

Following the procedure described for compound **17a** the title compound was obtained as yellow oil, 63.3% yield. The title compound was submitted to the following step without any further characterization.

4.1.20.   2-(1-Benzylpiperidin-4-yl)-2-(((8-hydroxyquinolin-2-yl)methyl)(prop-2-yn-1-yl)amino)acetonitrile (5d).

Following the procedure described for compound **5a** the title compound was obtained as yellow oil, 90% yield. IR ν_{max} = 2928, 2818, 2361, 2328, 1715, 1597, 1574, 1504, 1472, 1435, 1368, 1327, 1248,

35

1196, 1150, 1130, 1086, 988, 835, 758. ^{1}H NMR (400 MHz, CDCl$_3$), δ 8.11 (d, J = 8.4 Hz, 1H), 7.52 (d, J = 9.0 Hz, 1H), 7.42 (t, J = 7.8 Hz, 1H), 7.30-7.22 (m, 6H), 7.16 (d, J = 7.2 Hz, 1H), 4.24 (d, J = 14.4 Hz, 1H), 3.87 (d, J = 14.4 Hz, 1H), 3.55 (d, J = 13.6Hz, 2H), 3.49 (s, 1H), 3.43 (dd, J = 1.8 Hz, J = 16.8 Hz, 1H), 3.34 (dd, J = 2.4 Hz, J = 16.8 Hz, 1H), 2.94-2.88 (m, 2H), 2.31 (t, J = 2.4 Hz, 2H), 2.14-1.91 (m, 4H), 1.81-1.78 (m, 1H), 1.38-1.36 (m, 1H), 1.26-1.23 (m, 1H); ^{13}C NMR (150 MHz, CDCl$_3$), δ 155.8, 152.0, 137.4, 137.3, 137.1, 129.3, 128.3, 127.8, 127.6, 127.3, 121.3, 117.7, 116.3, 110.4, 78.6, 74.0, 62.9, 59.5, 57.4, 52.7, 52.6, 41.5, 36.6, 29.4, 29.2. HRMS (ESI): m/z [M + H]$^+$ calcd for C$_{27}$H$_{29}$N$_4$O: 425.2536; found 425.2335.

4.1.21. *3-(1-Benzylpiperidin-4-yl)-2-(((8-hydroxyquinolin-2-yl)methyl)(prop-2-yn-1-yl)amino)propanenitrile (5e)*

Following the procedure described for compound **5a** the title compound was obtained as yellow oil, 94.5% yield. IR ν$_{max}$ = 3287, 2936, 2799, 2768, 1711, 1601, 1574, 1505, 1474, 1452, 1368, 1327, 1248, 1150, 1129, 1088, 1028, 978, 910, 839, 741. ^{1}H NMR (400 MHz, CDCl$_3$), δ 8.05(d, J = 9.0 Hz, 1H), 7.46 (d, J = 8.4 Hz, 1H), 7.35(t, J = 7.8 Hz, 1H), 7.23-7.21 (m, 5H), 7.20-7.14 (m, 1H), 7.16 (dd, J = 1.2 Hz, J = 7.8 Hz, 1H), 4.17(d, J = 14.4 Hz, 1H), 3.93 (t, J = 7.8 Hz, 1H), 3.79 (d, J = 14.4 Hz, 1H), 3.39-3.29 (m, 3H), 3.29-3.26 (m, 1H), 2.81-2.76 (m, 2H), 2.50 (d, J = 1.2 Hz, 1H), 1.88-1.82 (m, 2H), 1.74-1.66 (m, 2H), 1.52-1.47 (m, 3H), 1.25-1.17 (m, 2H); ^{13}C NMR (150 MHz, CDCl$_3$), δ 155.9, 152.0, 138.3, 137.5, 137.0, 129.2, 128.2, 127.8, 127.1, 127.0, 121.4, 117.7, 117.4, 110.5, 78.5, 74.2, 63.3, 57.0, 53.4, 53.3, 53.0, 51.6, 41.5, 32.2, 32.0, 31.6. HRMS (ESI): m/z [M + H]$^+$ calcd for C$_{28}$H$_{31}$N$_4$O: 439.2492; found 439.2497.

4.1.21. *4-(1-Benzylpiperidin-4-yl)-2-(((8-hydroxyquinolin-2-yl)methyl)(prop-2-yn-1-yl)amino)butanenitrile (5f).*

Following the procedure described for compound **5a** the title compound was obtained as yellow oil, 91.8% yield. IR ν_{max} =3289, 2922, 2805, 2766, 1711, 1599, 1574, 1504, 1474, 1454, 1435, 1366, 1329, 1248, 1196, 1125, 1030, 980, 910, 839, 737. ^{1}H NMR (400 MHz, CDCl$_3$), δ 8.10 (d, J = 8.6 Hz, 1H), 7.53 (d, J = 8.6 Hz, 1H), 7.41 (t, J = 7.8 Hz, 1H), 7.28-7.26 (m, 5H), 7.22-7.20 (m, 1H), 7.15 (d, J = 7.8 Hz, 1H), 4.23 (d, J = 14.4 Hz, 1H), 3.88 (d, J = 13.8 Hz, 1H), 3.81 (t, J = 7.8 Hz, 1H), 3.46-3.42 (m, 3H), 3.36-3.33 (m, 1H), 2.81 (d, J = 10.8 Hz, 2H), 2.32 (d, J = 1.8 Hz, 1H), 2.13 (s, 3H), 1.84-1.81 (m, 4H), 1.57-1.54 (m, 2H), 1.39-1.37 (m, 2H), 1.22-1.18 (m, 3H); ^{13}C NMR (150 MHz, CDCl$_3$), δ 156.0, 152.0, 138.4, 137.4, 137.0, 129.2, 128.1, 127.7, 127.6, 126.9, 121.5, 117.7, 117.4, 110.4, 78.5, 74.2, 57.1, 54.1, 53.6, 41.4, 35.0, 32.5, 32.2, 32.0, 28.9. HRMS (ESI): m/z [M + H]$^+$ calcd for C$_{29}$H$_{33}$N$_4$O: 453.2649; found 453.2652.

4.2. In vitro biological assays.

4.2.1. Monoamine oxidase inhibition

Inhibition of *human recombinant* MAO-A and MAO-B (Sigma-Aldrich) by the selected derivatives was performed using a fluorometric method [53]. Enzymatic reactions took place in 96-well black opaque microplates (OptiPlate-96F, PerkinElmer) in a final volume of 200 µL. Serial dilutions of each inhibitor were pre-incubated for 30 min at 37 ˚C with 360 mU/mL MAO-A or 67.5 mU/mL MAO-B. Following the pre-incubations, enzymatic reactions were initiated by adding 100 µL of a mixture solution containing 1 mM *p*-tyramine as MAO substrate, 40 U/mL horseradish peroxidase (HRP) and 25 µM Amplex UltraRed™ reagent as final concentrations in 0.25 mM sodium phosphate (pH 7.4). The fluorescence production associated with peroxidase-coupled production of resorufin from Amplex UltraRed™ was continuously measured for at least one hour at λ_{530}(exc)/λ_{590}(em) in a spectrophotometric plate reader (FluoStar OPTIMA, BMG Labtech). Control experiments were carried out simultaneously by replacing the inhibitors by distilled water. In addition, the possible capacity of

compounds to modify the fluorescence generated in the reaction mixture due to non-enzymatic inhibition was determined by adding these compounds to solutions containing the Amplex UltraRed™ reagent only in phosphate buffer. Samples containing no substrate were used as blanks. Dose-response curves were plotted by using the GraphPad PRISM software (version 4.0) and IC_{50} values were accordingly calculated. Data were expressed as mean ± S.E.M. of at least three different experiments performed in triplicate.

4.2.2. Cholinesterases inhibition

ChEs inhibition was assessed following a spectrophometric method of Ellman [54] using *human recombinant* ChEs expressed in Hek293 cells (Sigma-Aldrich). Enzymatic reactions took place in 96-well plates in solutions containing 0.1 M phosphate buffer (pH 8.0), 0.035 U/mL AChE or 0.05 U/mL BuChE and 0.35 mM of 5,5'-dithiobis-2-nitrobenzoic acid (DTNB, Sigma-Aldrich). Inhibition curves were plotted by pre-incubating this mixture with serial dilutions of each compound for 30 min at 37 °C. The activity in absence of compound was used as control of the 100% of enzyme activity. After pre-incubation times, substrate was added to a final concentration of 0.35 mM acetylthiocholine iodide or 0.5 mM *S*-butyrylthiocholine iodide (Sigma-Aldrich) and enzymatic reactions were followed for at least 30 min. Changes in absorbance at λ_{405} were detected in a spectrophotometic plate reader (FluoStar OPTIMA, BMG Labtech) and IC_{50} values were calculated as the compound concentration inhibiting 50% of enzymatic activity by using the GraphPad PRISM software (version 4.0). Data were expressed as the mean ± S.E.M. of at least three different experiments performed in triplicate.

4.2.3. Assessment of reversibility and time-dependent inhibition

The reversibility of inhibition of *hr*MAO-A by **5f** was determined by measuring the recovery of enzymatic activity after a rapid and large dilution of the enzyme-compound complex. *hr*MAO-A was pre-incubated for 30 min at 100-fold over the concentration required for the activity assay with 100 μM

38

5f or 200 nM clorgyline, as an irreversible standard compound, corresponding to 10-fold of IC_{50} value previously determined. The mixture was diluted 100-fold into reaction buffer containing 1 mM *p*-tyramine. The progress curves were measured at λ_{405} and compared to that of samples with no inhibitor. Time-dependent inhibition of *hr*MAO-A by **5f** was evaluated by carrying out several pre-incubations (0-240 min) of increasing concentrations of the inhibitor with the enzyme. Dose-response curves (IC_{50}) were determined accordingly for each pre-incubation as previously described.

4.2.4. Cholinesterase kinetic assessment

To assess the mechanism of action of **5f** inhibiting both *hr*ChEs (AChE and BuChE), reciprocal plots of 1/V versus 1/[S] were determined using substrate concentrations ranging 0.1-2 mM of acetylthiocholine iodide (ASCh) or *S*-butyrylthiocholine iodide (BuSCh), respectively. Enzyme activity was determined by using the Ellman's method [54], adding enzyme at last. The plots were assessed by a weighted least-squares analysis and slopes of reciprocal plots were plotted against **5f** concentration (0-200 nM). Inhibition constants (Ki) were estimated using the non-linear analysis method.

4.2.5. Assessment of metal-chelating properties

Complexing studies were performed in distilled water at room temperature using a UV-VIS spectrophotometer (Lambda25, PerkinElmer). Spectral changes (220-300 nm) of 10 µM **5f** in presence of metals $CuSO_4$, $Fe_2(SO)_3$ and $ZnSO_4$ at concentrations ranging 1-5 µM of were detected in 1cm-quartz cells. The stoichiometry of the complexes **5f**-Cu(II)/Zn(II) was determined using the Job's method [55]. Briefly, 21 different solutions containing **5f** and biometals $CuSO_4$ and $ZnSO_4$ were prepared at a final sum of concentrations of both species of 10 µM, varying the proportions of both components between 0 and 100%. Absorbance at 262 nm was plotted versus the mole fraction of **5f** for each metal.

4.2.6. Evaluation of antioxidant properties of 5f

4.2.6.1. Inhibition of lipid peroxidation (LPO)

Production of conjugated diene hydroperoxide by oxidation of linoleic acid in an aqueous dispersion was monitored at 234 nm as previously described [56]. AAPH was used as a free radical initiator. 10 µL of 16 mM linoleic acid dispersion were added to the UV cuvette containing 0.93 mL of 0.05 M phosphate buffer pH 7.4 at 37 °C. The oxidation reaction was initiated upon the addition of 50 mL of 40 mM AAPH solution. Oxidation was carried out in the presence of aliquots (10 mL) in the assay without antioxidant; lipid oxidation was measured in the presence of the same level of DMSO. The rate of oxidation at 37 °C was monitored by recording the increase in absorption at 234 nm caused by conjugated diene hydroperoxides.

4.2.6.2. Oxygen Radical Absorbance Capacity (ORAC) assay

The ORAC assay was performed as previously described [57]. Briefly, AAPH was used as free radical generator and trolox as standard while melatonin was used as a reference compound (both compounds, Sigma-Aldrich). Compounds 5f and melatonin were diluted in 75 mM PBS pH 7.4 and measured at different concentrations (0.1-1 µM). Trolox calibration was used for the standard curve. Samples were pre-incubated for 15 min at 37 °C with 70 nM fluorescein (Sigma-Aldrich). Upon the addition of 12 mM AAPH, the fluorescence intensity ($\lambda_{exc} = 485$ nm, $\lambda_{em} = 520$ nm) was monitored every minute for 1 h using a Polarstar Galaxy plate reader (BMG Labtechnologies GmbH). The area under the curve (AUC) of the fluorescence decay was calculated by subtracting AUC values for the same sample or standard from that for the net AUC values of trolox standard solutions. The ORAC value for each tested compound was expressed as trolox equivalent (µmol of trolox/µmol of compound). The ORAC value for trolox was assigned as 1.

4.2.6.3. Determination of the reducing activity of the stable radical DPPH

As previously reported [58], to a solution of 0.1 mM DPPH in absolute EtOH, an equal volume of the compounds, dissolved in DMSO, was added. The mixture was vigorously shaken and allowed to stand for 60 min. Then, absorbance at 517 nm was determined spectrophotometrically and the % of activity was calculated. All tests were undertaken on three replicates and the results were averaged.

4.2.6.4. Induction of H_2O_2 by Cu(II) and ascorbic acid

The production H_2O_2 was induced *in vitro* by incubating 0.2 μM Cu(II), 10 μM ascorbic acid (Sigma-Aldrich). Following an incubation of 10 min at rt with different concentrations of **5f**, a mixture containing horseradish peroxidase and Amplex Red reagent was added to quantify the amount of H_2O_2 produced. Distilled water was used to determine the maximum levels of H_2O_2.

4.3. Molecular Modeling

All calculations performed in this work were carried out on Cooler Master Centurion 5 (Intel Core i5–2500 CPU @ 3.30 GHz Quad) with Ubuntu 10.04 LTS (long-term support) operating system running Maestro 9.3 (Schrödinger, LLC, New York, NY, 2012).

4.3.1. Proteins and Ligands preparation

The three-dimensional structure of the *human* MAO-A, MAO-B and AChE enzymes were taken from PDB (ID 2Z5X, 2V5Z, and 1B41, respectively). The co-crystallized ligands, compounds used for solving the structures and molecules of water were removed from the proteins and the resulting structures were submitted to protein preparation wizard implemented in Maestro suite 2012 (Protein Preparation Wizard workflow 2012; http://www.schrodinger.com/supportdocs/18/16). Three-dimensional structure building for all compounds in this study was carried out by means of Maestro [42]. Molecular energy minimizations were performed in MacroModel [59] using the Optimized

41

Potentials for Liquid Simulations-all atom (OPLS-AA) force field 2005 [60, 61]. The solvent effects are simulated using the analytical Generalized-Born/Surface-Area (GB/SA) model [62], and no cutoff for nonbonded interactions was selected. Polak-Ribiere conjugate gradient (PRCG) method with 1000 maximum iterations and 0.001 gradient convergence threshold was employed. All compounds reported in this paper were prepared taking into account the protonation state reported in Table S1 calculated by means of ACDlabs (ACD/pKa DB software, version 12.00; Advanced Chemistry Development, Inc., Toronto, Canada).

4.3.2. Induced Fit Docking (IFD)

Molecular docking was carried out using the Schrödinger suite 2012 by applying the IFD protocol [63]. This procedure induces conformational changes in the binding site to accommodate the ligand and exhaustively identify possible binding modes and associated conformational changes by side-chain sampling and backbone minimization. The proteins and the ligands used in this step were prepared as reported in the previous paragraphs. The boxes for docking calculation was built starting from the crystallized non-covalent inhibitors for MAO enzymes, while for *h*AChE from the centre of the gorge selecting the residues Asp74 as previously reported [31, 32]. IFD includes protein side-chain flexibility in a radius of 5.0 Å around the poses found during the initial docking stage of the IFD protocol. Complexes within 30.0 kcal/mol of minimum energy structure were taken forward for redocking. The Glide redocking stage was performed by XP (Extra Precision) methods. The calculations were performed using default IFD protocol parameters. No hydrogen bonding or other constraints were used.

4.3.3. Estimated free-binding energies

The Prime/MM-GBSA method implemented in Prime software [64] consists in computing the change between the free and the complex state of both the ligand and the protein after energy minimization.

42

The technique was used on the docking complexes herein reported. The software was used to calculate the free-binding energy (ΔG_{bind}) as previously reported [33, 46, 65-67].

4.3.4. Predicted physicochemical properties

QikProp application [48] was used for predicting the physicochemical properties of compounds presented in this study.

Acknowledgments

Supplementary Material

Supplementary data associated with this article (Table S1 and Figures S1,S2) can be found, in the online version, at….

References

[1] A. Burns, S. Iliffe, Dementia, BMJ, 338 (2009) b75.

[2] H.W. Querfurth, F.M. LaFerla, Alzheimer's disease, N. Engl. J. Med., 362 (2010) 329-344.

[3] D.S. Auld, T.J. Kornecook, S. Bastianetto, R. Quirion, Alzheimer's disease and the basal forebrain cholinergic system: relations to beta-amyloid peptides, cognition, and treatment strategies, Prog. Neurobiol., 68 (2002) 209-245.

[4] J. Hardy, The amyloid hypothesis for Alzheimer's disease: a critical reappraisal, J. Neurochem., 110 (2009) 1129-1134.

[5] A. Gella, N. Durany, Oxidative stress in Alzheimer disease, Cell Adhes. Migrat., 3 (2009) 88-93.

[6] D.J. Selkoe, Alzheimer's disease results from the cerebral accumulation and cytotoxicity of amyloid beta-protein, J. Alzheimers Dis., 3 (2001) 75-80.

[7] WHO, Dementia: a public health priority, in: http://www.who.int/mental_health/publications/dementia_report_2012/en/, 2012.

[8] K. Blennow, M.J. de Leon, H. Zetterberg, Alzheimer's disease, Lancet, 368 (2006) 387-403.

[9] G. Pepeu, M.G. Giovannini, Cholinesterase inhibitors and beyond, Curr. Alzheimer Res., 6 (2009) 86-96.

[10] J.L. Cummings, Treatment of Alzheimer's disease: current and future therapeutic approaches, Rev. Neurol. Dis., 1 (2004) 60-69.

[11] J.B. Standridge, Pharmacotherapeutic approaches to the prevention of Alzheimer's disease, Am. J. Geriatr. Pharmacother., 2 (2004) 119-132.

[12] N. Qizilbash, J. Birks, J. Lopez Arrieta, S. Lewington, S. Szeto, WITHDRAWN: Tacrine for Alzheimer's disease, The Cochrane database of systematic reviews, (2007) CD000202.

[13] P.B. Watkins, H.J. Zimmerman, M.J. Knapp, S.I. Gracon, K.W. Lewis, Hepatotoxic effects of tacrine administration in patients with Alzheimer's disease, JAMA, 271 (1994) 992-998.

45

[14] D. Lagadic-Gossmann, M. Rissel, M.A. Le Bot, A. Guillouzo, Toxic effects of tacrine on primary hepatocytes and liver epithelial cells in culture, Cell Biol. Toxicol., 14 (1998) 361-373.

[15] C. Mount, C. Downton, Alzheimer disease: progress or profit?, Nat. Med., 12 (2006) 780-784.

[16] L. Pisani, M. Catto, F. Leonetti, O. Nicolotti, A. Stefanachi, F. Campagna, A. Carotti, Targeting monoamine oxidases with multipotent ligands: an emerging strategy in the search of new drugs against neurodegenerative diseases, Curr. Med. Chem., 18 (2011) 4568-4587.

[17] M. Sadowski, T. Wisniewski, Disease modifying approaches for Alzheimer's pathology, Curr. Pharm. Des., 13 (2007) 1943-1954.

[18] M.S. Song, D. Matveychuk, E.M. MacKenzie, M. Duchcherer, D.D. Mousseau, G.B. Baker, An update on amine oxidase inhibitors: multifaceted drugs, Prog. Neuropsychopharmacol. Biol. Psychiatry, 44 (2013) 118-124.

[19] J.P. Finberg, Update on the pharmacology of selective inhibitors of MAO-A and MAO-B: focus on modulation of CNS monoamine neurotransmitter release, Pharmacol. Ther., 143 (2014) 133-152.

[20] T. Storr, K.H. Thompson, C. Orvig, Design of targeting ligands in medicinal inorganic chemistry, Chem. Soc. Rev., 35 (2006) 534-544.

[21] M.P. Cuajungco, K.Y. Faget, Zinc takes the center stage: its paradoxical role in Alzheimer's disease, Brain Res. Brain Res. Rev., 41 (2003) 44-56.

[22] D.D. Thomas, L.A. Ridnour, J.S. Isenberg, W. Flores-Santana, C.H. Switzer, S. Donzelli, P. Hussain, C. Vecoli, N. Paolocci, S. Ambs, C.A. Colton, C.C. Harris, D.D. Roberts, D.A. Wink, The chemical biology of nitric oxide: implications in cellular signaling, Free Radic. Biol. Med., 45 (2008) 18-31.

[23] T. Korcsmaros, M.S. Szalay, C. Bode, I.A. Kovacs, P. Csermely, How to design multi-target drugs, Exp. Op. Drug Disc., 2 (2007) 799-808.

[24] A. Cavalli, M.L. Bolognesi, S. Capsoni, V. Andrisano, M. Bartolini, E. Margotti, A. Cattaneo, M. Recanatini, C. Melchiorre, A small molecule targeting the multifactorial nature of Alzheimer's disease, Angew. Chem. Int. Ed. Engl., 46 (2007) 3689-3692.

[25] M.B. Youdim, J.J. Buccafusco, Multi-functional drugs for various CNS targets in the treatment of neurodegenerative disorders, Trends Pharmacol. Sci., 26 (2005) 27-35.

[26] M.L. Bolognesi, A. Cavalli, L. Valgimigli, M. Bartolini, M. Rosini, V. Andrisano, M. Recanatini, C. Melchiorre, Multi-target-directed drug design strategy: from a dual binding site acetylcholinesterase inhibitor to a trifunctional compound against Alzheimer's disease, J. Med. Chem., 50 (2007) 6446-6449.

[27] P. Camps, X. Formosa, C. Galdeano, T. Gomez, D. Munoz-Torrero, L. Ramirez, E. Viayna, E. Gomez, N. Isambert, R. Lavilla, A. Badia, M.V. Clos, M. Bartolini, F. Mancini, V. Andrisano, A. Bidon-Chanal, O. Huertas, T. Dafni, F.J. Luque, Tacrine-based dual binding site acetylcholinesterase inhibitors as potential disease-modifying anti-Alzheimer drug candidates, Chem. Biol. Interact., 187 (2010) 411-415.

[28] P. Camps, X. Formosa, C. Galdeano, D. Munoz-Torrero, L. Ramirez, E. Gomez, N. Isambert, R. Lavilla, A. Badia, M.V. Clos, M. Bartolini, F. Mancini, V. Andrisano, M.P. Arce, M.I. Rodriguez-Franco, O. Huertas, T. Dafni, F.J. Luque, Pyrano[3,2-c]quinoline-6-chlorotacrine hybrids as a novel family of acetylcholinesterase- and beta-amyloid-directed anti-Alzheimer compounds, J. Med. Chem., 52 (2009) 5365-5379.

[29] S. Butini, G. Campiani, M. Borriello, S. Gemma, A. Panico, M. Persico, B. Catalanotti, S. Ros, M. Brindisi, M. Agnusdei, I. Fiorini, V. Nacci, E. Novellino, T. Belinskaya, A. Saxena, C. Fattorusso, Exploiting protein fluctuations at the active-site gorge of human cholinesterases: further optimization of the design strategy to develop extremely potent inhibitors, J. Med. Chem., 51 (2008) 3154-3170.

[30] G. Campiani, C. Fattorusso, S. Butini, A. Gaeta, M. Agnusdei, S. Gemma, M. Persico, B. Catalanotti, L. Savini, V. Nacci, E. Novellino, H.W. Holloway, N.H. Greig, T. Belinskaya, J.M. Fedorko, A. Saxena, Development of molecular probes for the identification of extra interaction sites in the mid-gorge and peripheral sites of butyrylcholinesterase (BuChE). Rational design of novel, selective, and highly potent BuChE inhibitors, J. Med. Chem., 48 (2005) 1919-1929.

[31] M. Chioua, M. Perez, O.M. Bautista-Aguilera, M. Yanez, M.G. Lopez, A. Romero, R. Cacabelos, R.P. de la Bellacasa, S. Brogi, S. Butini, J.I. Borrell, J. Marco-Contelles, Development of HuperTacrines as Non-Toxic, Cholinesterase Inhibitors for the Potential Treatment of Alzheimer's Disease, Mini Rev. Med. Chem.;15(8) (2015) 648-658.

[32] S. Butini, M. Brindisi, S. Brogi, S. Maramai, E. Guarino, A. Panico, A. Saxena, V. Chauhan, R. Colombo, L. Verga, E. De Lorenzi, M. Bartolini, V. Andrisano, E. Novellino, G. Campiani, S. Gemma, Multifunctional Cholinesterase and Amyloid Beta Fibrillization Modulators. Synthesis and Biological Investigation, ACS Med. Chem. Lett., 4 (2013) 1178-1182.

[33] S. Brogi, S. Butini, S. Maramai, R. Colombo, L. Verga, C. Lanni, E. De Lorenzi, S. Lamponi, M. Andreassi, M. Bartolini, V. Andrisano, E. Novellino, G. Campiani, M. Brindisi, S. Gemma, Disease-modifying anti-Alzheimer's drugs: inhibitors of human cholinesterases interfering with beta-amyloid aggregation, CNS Neurosci. Ther., 20 (2014) 624-632.

[34] O.M. Bautista-Aguilera, A. Samadi, M. Chioua, K. Nikolic, S. Filipic, D. Agbaba, E. Soriano, L. de Andres, M.I. Rodriguez-Franco, S. Alcaro, R.R. Ramsay, F. Ortuso, M. Yanez, J. Marco-Contelles, N-Methyl-N-((1-methyl-5-(3-(1-(2-methylbenzyl)piperidin-4-yl)propoxy)-1H-indol-2- yl)methyl)prop-2-yn-1-amine, a new cholinesterase and monoamine oxidase dual inhibitor, J. Med. Chem., 57 (2014) 10455-10463.

[35] O.M. Bautista-Aguilera, G. Esteban, M. Chioua, K. Nikolic, D. Agbaba, I. Moraleda, I. Iriepa, E. Soriano, A. Samadi, M. Unzeta, J. Marco-Contelles, Multipotent cholinesterase/monoamine oxidase

inhibitors for the treatment of Alzheimer's disease: design, synthesis, biochemical evaluation, ADMET, molecular modeling, and QSAR analysis of novel donepezil-pyridyl hybrids, Drug Des. Dev. Ther., 8 (2014) 1893-1910.

[36] M.G. Kallitsakis, M. Yanez, E. Soriano, J. Marco-Contelles, D.J. Hadjipavlou-Litina, K.E. Litinas, Purine homo-N-nucleoside+coumarin hybrids as pleiotropic agents for the potential treatment of Alzheimer's disease, Future Med. Chem., 7 (2015) 103-110.

[37] M. Benchekroun, L. Ismaili, M. Pudlo, V. Luzet, T. Gharbi, B. Refouvelet, J. Marco-Contelles, Donepezil-ferulic acid hybrids as anti-Alzheimer drugs, Future medicinal chemistry, 7 (2015) 15-21.

[38] L. Wang, G. Esteban, M. Ojima, O.M. Bautista-Aguilera, T. Inokuchi, I. Moraleda, I. Iriepa, A. Samadi, M.B. Youdim, A. Romero, E. Soriano, R. Herrero, A.P. Fernandez Fernandez, M. Ricardo Martinez, J. Marco-Contelles, M. Unzeta, Donepezil + propargylamine + 8-hydroxyquinoline hybrids as new multifunctional metal-chelators, ChE and MAO inhibitors for the potential treatment of Alzheimer's disease, Eur. J. Med. Chem., 80 (2014) 543-561.

[39] S. Mann, S. Carillon, O. Breyne, A. Marquet, Total synthesis of amiclenomycin, an inhibitor of biotin biosynthesis, Chemistry, 8 (2002) 439-450.

[40] S. Butini, E. Guarino, G. Campiani, M. Brindisi, S.S. Coccone, I. Fiorini, E. Novellino, T. Belinskaya, A. Saxena, S. Gemma, Tacrine based human cholinesterase inhibitors: synthesis of peptidic-tethered derivatives and their effect on potency and selectivity, Bioorg. Med. Chem. Lett., 18 (2008) 5213-5216.

[41] Schrödinger Suite 2012 Induced Fit Docking protocol; Glide version 5.8, Schrödinger, LLC, New York, NY, 2012; Prime version 3.1, Schrödinger, LLC, New York, NY, 2012.

[42] Maestro, version 9.3, Schrödinger, LLC, New York, NY, 2012.

[43] S. Gemma, C. Camodeca, M. Brindisi, S. Brogi, G. Kukreja, S. Kunjir, E. Gabellieri, L. Lucantoni, A. Habluetzel, D. Taramelli, N. Basilico, R. Gualdani, F. Tadini-Buoninsegni, G.

Bartolommei, M.R. Moncelli, R.E. Martin, R.L. Summers, S. Lamponi, L. Savini, I. Fiorini, M. Valoti, E. Novellino, G. Campiani, S. Butini, Mimicking the intramolecular hydrogen bond: synthesis, biological evaluation, and molecular modeling of benzoxazines and quinazolines as potential antimalarial agents, J. Med. Chem., 55 (2012) 10387-10404.

[44] M. Anzini, A. Di Capua, S. Valenti, S. Brogi, M. Rovini, G. Giuliani, A. Cappelli, S. Vomero, L. Chiasserini, A. Sega, G. Poce, G. Giorgi, V. Calderone, A. Martelli, L. Testai, L. Sautebin, A. Rossi, S. Pace, C. Ghelardini, L. Di Cesare Mannelli, V. Benetti, A. Giordani, P. Anzellotti, M. Dovizio, P. Patrignani, M. Biava, Novel analgesic/anti-inflammatory agents: 1,5-diarylpyrrole nitrooxyalkyl ethers and related compounds as cyclooxygenase-2 inhibiting nitric oxide donors, J. Med. Chem., 56 (2013) 3191-3206.

[45] A. Cappelli, M. Manini, S. Valenti, F. Castriconi, G. Giuliani, M. Anzini, S. Brogi, S. Butini, S. Gemma, G. Campiani, G. Giorgi, L. Mennuni, M. Lanza, A. Giordani, G. Caselli, O. Letari, F. Makovec, Synthesis and structure-activity relationship studies in serotonin 5-HT1A receptor agonists based on fused pyrrolidone scaffolds, Eur. J. Med. Chem., 63 (2013) 85-94.

[46] S. Giovani, M. Penzo, S. Brogi, M. Brindisi, S. Gemma, E. Novellino, L. Savini, M.J. Blackman, G. Campiani, S. Butini, Rational design of the first difluorostatone-based PfSUB1 inhibitors, Bioorg. Med. Chem. Lett., 24 (2014) 3582-3586.

[47] S.Y. Son, J. Ma, Y. Kondou, M. Yoshimura, E. Yamashita, T. Tsukihara, Structure of human monoamine oxidase A at 2.2-A resolution: the control of opening the entry for substrates/inhibitors, Proc. Natl. Acad. Sci. U.S.A., 105 (2008) 5739-5744.

[48] QikProp, version 3.5, Schrödinger, LLC, New York, NY, 2012.

[49] A.I. Bush, The metal theory of Alzheimer's disease, J. Alzheimers Dis., 33 Suppl 1 (2013) S277-281.

[50] D.J. Bonda, X. Wang, G. Perry, A. Nunomura, M. Tabaton, X. Zhu, M.A. Smith, Oxidative stress in Alzheimer disease: a possibility for prevention, Neuropharmacol., 59 (2010) 290-294.

[51] P.W. Mantyh, J.R. Ghilardi, S. Rogers, E. DeMaster, C.J. Allen, E.R. Stimson, J.E. Maggio, Aluminum, iron, and zinc ions promote aggregation of physiological concentrations of beta-amyloid peptide, J. Neurochem., 61 (1993) 1171-1174.

[52] F. Hane, Z. Leonenko, Effect of metals on kinetic pathways of amyloid-beta aggregation, Biomolecules, 4 (2014) 101-116.

[53] M. Zhou, N. Panchuk-Voloshina, A one-step fluorometric method for the continuous measurement of monoamine oxidase activity, Anal. Biochem., 253 (1997) 169-174.

[54] G.L. Ellman, K.D. Courtney, V. Andres, Jr., R.M. Feather-Stone, A new and rapid colorimetric determination of acetylcholinesterase activity, Biochem. Pharmacol., 7 (1961) 88-95.

[55] C.Y. Huang, Determination of binding stoichiometry by the continuous variation method: the Job plot, Methods Enzymol., 87 (1982) 509-525.

[56] M. Chioua, D. Sucunza, E. Soriano, D. Hadjipavlou-Litina, A. Alcazar, I. Ayuso, M.J. Oset-Gasque, M.P. Gonzalez, L. Monjas, M.I. Rodriguez-Franco, J. Marco-Contelles, A. Samadi, Alpha-aryl-N-alkyl nitrones, as potential agents for stroke treatment: synthesis, theoretical calculations, antioxidant, anti-inflammatory, neuroprotective, and brain-blood barrier permeability properties, J. Med. Chem., 55 (2012) 153-168.

[57] A. Davalos, C. Gomez-Cordoves, B. Bartolome, Extending applicability of the oxygen radical absorbance capacity (ORAC-fluorescein) assay, J. Agric. Food Chem., 52 (2004) 48-54.

[58] T. Symeonidis, M. Chamilos, D.J. Hadjipavlou-Litina, M. Kallitsakis, K.E. Litinas, Synthesis of hydroxycoumarins and hydroxybenzo[f]- or [h]coumarins as lipid peroxidation inhibitors, Bioorg. Med. Chem. Lett., 19 (2009) 1139-1142.

[59] MacroModel, version 9.9, Schrödinger, LLC, New York, NY, 2012.

[60] W.L. Jorgensen, D.S. Maxwell, J. TiradoRives, Development and testing of the OPLS all atom force field on conformational energetics and properties of organic liquids J. Am. Chem. Soc., 118 (1996) 11225-11236.

[61] G.A. Kaminski, R.A. Friesner, J. Tirado-Rives, W.L. Jorgensen, Evaluation and reparametrization of the OPLS-AA force field for proteins via comparison with accurate quantum chemical calculations on peptides, J. Phys. Chem. B, 105 (2001) 6474-6487.

[62] W.C. Still, A. Tempczyk, R.C. Hawley, T. Hendrickson, Semianalytical Treatment of Solvation for Molecular Mechanics and Dynamics, J. Am. Chem. Soc., 112 (1990) 6127-6129.

[63] W. Sherman, T. Day, M.P. Jacobson, R.A. Friesner, R. Farid, Novel procedure for modeling ligand/receptor induced fit effects, Journal of medicinal chemistry, 49 (2006) 534-553.

[64] Prime, version 3.1, Schrödinger, LLC, New York, NY, 2012.

[65] M. Brindisi, S. Gemma, S. Kunjir, L. Di Cerbo, S. Brogi, S. Parapini, S. D'Alessandro, D. Taramelli, A. Habluetzel, S. Tapanelli, S. Lamponi, E. Novellino, G. Campiani, S. Butini, Synthetic spirocyclic endoperoxides: new antimalarial scaffolds, Med. Chem. Commun., 6 (2015) 357-362.

[66] S. Giovani, M. Penzo, S. Butini, M. Brindisi, S. Gemma, E. Novellino, G. Campiani, M. Blackman, S. Brogi, Plasmodium falciparum Subtilisin-like Protease 1: Discovery of Potent Difluorostatone-based Inhibitors, RSC Adv., 5(29) (2015) 22431-22448.

[67] M. Brindisi, S. Butini, S. Franceschini, S. Brogi, F. Trotta, S. Ros, A. Cagnotto, M. Salmona, A. Casagni, M. Andreassi, S. Saponara, B. Gorelli, P. Weikop, J.D. Mikkelsen, J. Scheel-Kruger, K. Sandager-Nielsen, E. Novellino, G. Campiani, S. Gemma, Targeting Dopamine D3 and Serotonin 5-HT1A and 5-HT2A Receptors for Developing Effective Antipsychotics: Synthesis, Biological Characterization, and Behavioral Studies, J. Med. Chem., 57 (2014) 9578-9597.

Graphical Abstract

Donepezil-like Multifunctional Agents: Design, Synthesis, Molecular Modeling and Biological Evaluation

Ming-Yu Wu,[§] Gerard Esteban,[§] Simone Brogi,[§] Masahi Shionoya, Li Wang, Giuseppe Campiani, Mercedes Unzeta,[*] Tsutomu Inokuchi,[*] Stefania Butini,[*] and Jose Marco-Contelles[*]

[§]Authors equally contributed to this work
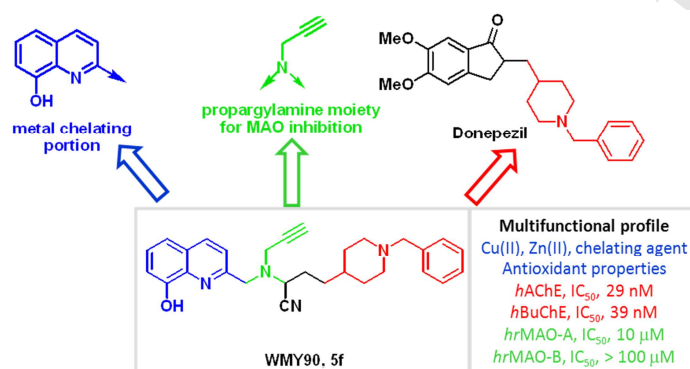
Highlights

- Development of multifunctional compounds
- Potential therapeutic agents for the treatment of AD
- Scaffold hopping approach

Running Title

Multifunctional Agents as Potential AD Therapeutics

Supplementary Material

Donepezil-like Multifunctional Agents: Design, Synthesis, Molecular Modeling and Biological Evaluation

Ming-Yu Wu,[a,§] Gerard Esteban,[b,§] Simone Brogi,[c,§] Masahi Shionoya,[a] Li Wang,[a] Giuseppe Campiani,[c] Mercedes Unzeta,[b,*] Tsutomu Inokuchi,[a,*] Stefania Butini,[c,*] and Jose Marco-Contelles[d,*]

[a]*Division of Chemistry and Biotechnology, Graduate School of Natural Science and Technology, Okayama University, 3.1.1 Tsushima-Naka, Kita-ku, Okayama 700-8530, Japan.*

[b]*Departament de Bioquímica i Biologia Molecular, Facultat de Medicina, Institut de Neurociències, Universitat Autònoma de Barcelona, 08193 Bellaterra, Barcelona, Spain.*

[c]*European Research Centre for Drug Discovery and Development (NatSynDrugs) and Department of Biotechnology, Chemistry and Pharmacy, Università degli Studi di Siena Via A. Moro, 53100 Siena, Italy.*

[d]*Laboratory of Medicinal Chemistry (IQOG, CSIC), C/Juan de la Cierva 3, 28006-Madrid, Spain.*

[*]Corresponding author. Tel. +34 93 5811523; fax +34 935811573; e-mail: mercedes.unzeta@uab.cat
[*]Corresponding author. Tel. +81862945045; fax +81862518021; e-mail: inokuchi@cc.okayama-u.ac.jp
[*]Corresponding author. Tel.: +39 0577234161; fax: +39 0577 234254; e-mail: butini3@unisi.it
[*]Corresponding author. Tel.: + 34 915622900; fax: +39 915644853; e-mail: iqoc21@iqog.csic.es
[§]Authors equally contributed to this work

Table of Contents

Table S1. Calculated protonation state at physiological pH (7.4)[a] for compounds presented in this study.

Compound	Structure	Protonation State
5a		**N10+, N18+, 30-** 83% **N18+** 9%
5b		**N10+, N20+, 17-** 86% **N20+** 10.1%
5c		**N10+, N21+, 17-** 86.7% **N21+** 10%
5d		**N10+, N18+, 30-** 74.2% **N10+, 30-** 18.6% **N18+** 5.4%
5e		**N10+, N20+, 17-** 85.7% **N20+** 8.6% **N10+, 17-** 4.5%
5f		**N10+, N21+, 17-** 82% **N21+** 14% **N10+, 17-** 2.8%

[a]All values were calculated by means of ACDlabs software package (ACD/pKa DB software, version 12.00; Advanced Chemistry Development, Inc., Toronto, Canada).
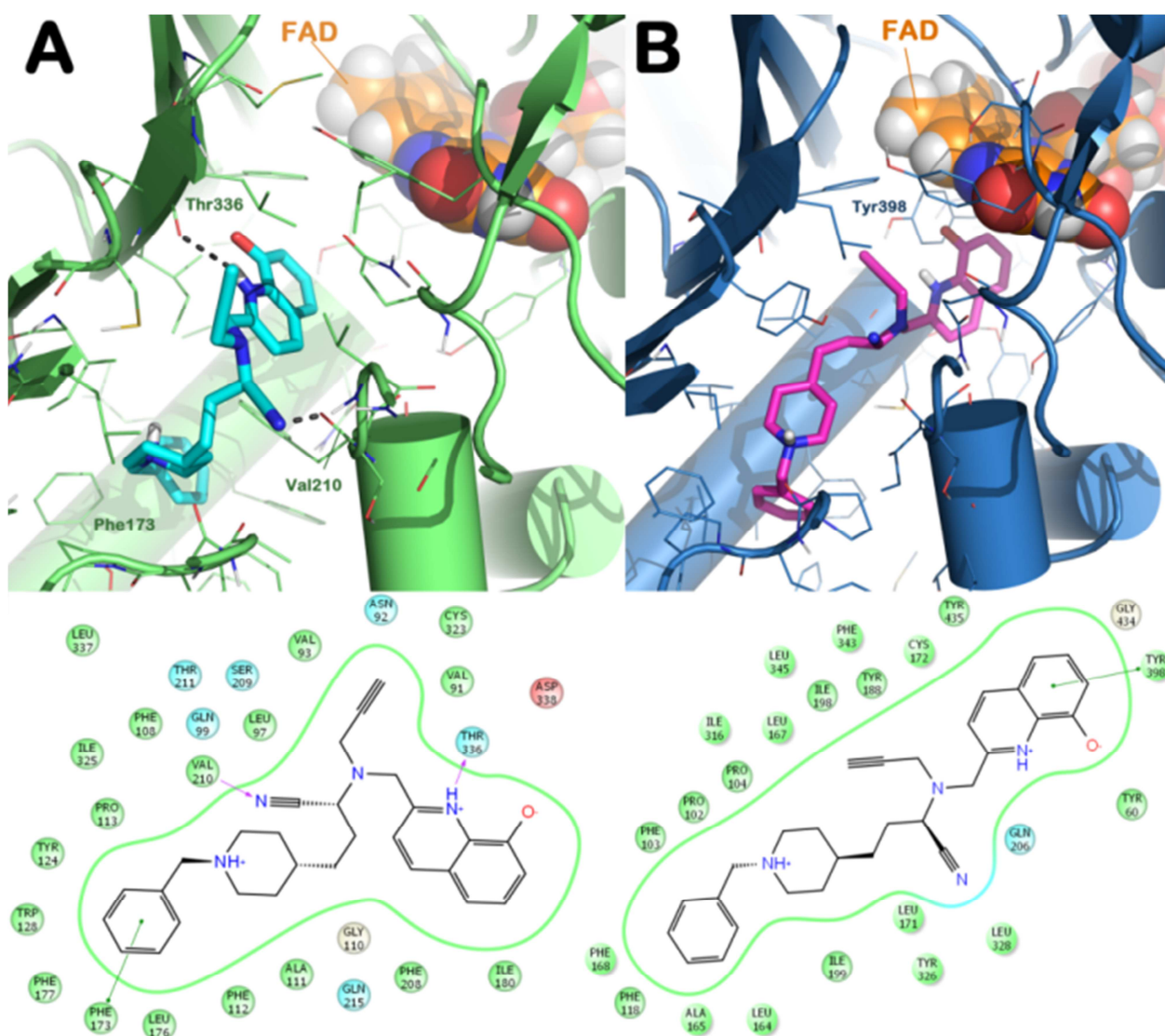
Figure S1. Docked pose of **5f** *R*-enantiomer into *h*MAO A (PDB ID: 2Z5X) binding site, while in the bottom part of the picture is represented schematic ligand-protein interaction. (B) Docked pose of **5f** *R*-enantiomer into *h*MAO B (PDB ID: 2V5Z) binding site, while in the bottom part of the picture is represented schematic ligand-protein interaction. The docked poses are visualized by means of PyMOL (PyMOL is an OPEN SOURCE program distributed under the "Python" license. The PyMOL Molecular Graphics System, v1.6-alpha; Schrodinger LLC, New York, NY, 2013), while the ligand-protein interaction diagram was generated by means of Maestro (Maestro; version 9.3, Schrödinger, LLC, New York, NY, 2012).
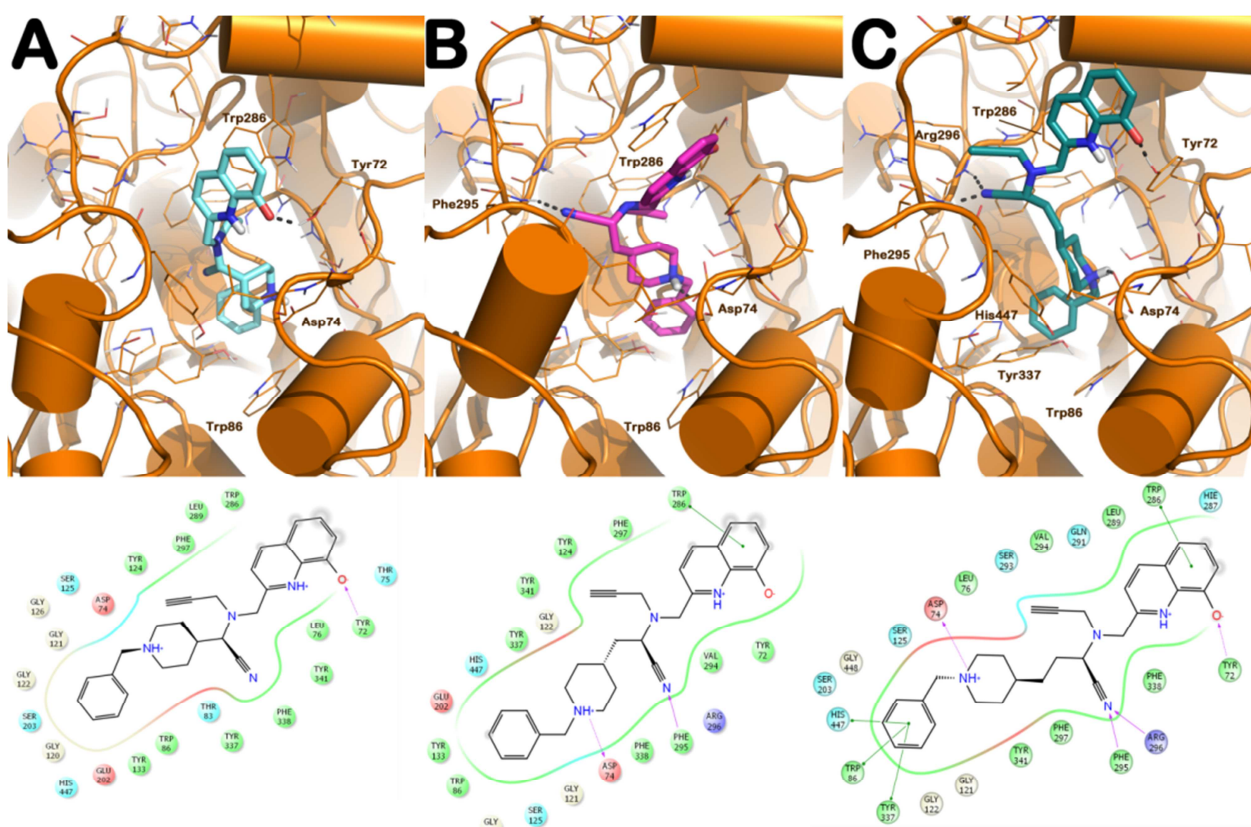
Figure S2. Docked poses of **5d** (A), **5e** (B), **5f** (C) *R*-enantiomers into *h*AChE binding site (PDB ID: 1B41), while in the bottom part of the picture is represented a schematic ligand-protein interactions.